Chemical Geology 353 (2013) 230–245

Contents lists available at ScienceDirect

Chemical Geology

journal homepage: www.elsevier.com/locate/chemgeo

Calc-alkaline lamprophyres from Lusatia (Germany)—Evidence for a repeatedly enriched mantle source

Kh.M. Abdelfadil [a,*], R.L. Romer [a], Th. Seifert [b], R. Lobst [c]

[a] Deutsches GeoForschungZentrum (GFZ), Telegrafenberg, D-14473 Potsdam, Germany
[b] TU Bergakademie Freiberg, Division of Economic Geology and Petrology, Brennhausgasse 14, D-09596 Freiberg, Germany
[c] Sächsisches Landesamt für Umwelt, Landwirtschaft und Geologie Pillnitzer Platz 3, D-01326 Dresden, Germany

ARTICLE INFO

Article history:
Accepted 8 October 2012
Available online 16 October 2012

Keywords:
Tholeiitic gabbro
Spessartite
Mantle metasomatism
Variscan orogeny

ABSTRACT

Pre-Variscan mantle derived gabbros (c. 400 Ma) and late-Variscan calc-alkaline lamprophyres (c. 330 Ma) were emplaced within the Cadomian basement of Lusatia. They were sampled to characterize the effect of the Variscan orogeny onto the mantle beneath Lusatia. The tholeiitic gabbros originated from a mantle source that had been metasomatized during subduction beneath the Cadomian magmatic arc at c. 570 Ma, which led to enrichment of LREE, Ba/Nb, and LILE relative to primitive mantle. The late-Variscan calc-alkaline lamprophyres (spessartites) have high MgO, Cr, and Ni contents reflecting the mantle source. The spessartites, however, have distinctly higher Rb, Ba, Pb, Sr, Th, and Cs contents, higher La/Yb, $^{87}Sr/^{86}Sr$, and $^{206}Pb/^{204}Pb$ ratios, and lower $^{143}Nd/^{144}Nd$ ratios than the gabbros, which indicates a second, Variscan event of mantle enrichment. In addition, the spessartites have trace element ratios (i.e., Ba/Nb, Nb/U, Th/U, and Th/Nb) that resemble continental crust and Sr, Nd, and Pb isotopic compositions that demonstrate involvement of crustal material by source enrichment during the Variscan orogeny. The calc-alkaline lamprophyres of the Lusatia occupy the same age range as calc-alkaline lamprophyres from the adjacent Erzgebirge and Sudetes. The trace-element signatures and Sr and Nd isotopic compositions of Lusatian spessartites, however, are less enriched than those of comparable dikes in the Sudetes and the Erzgebirge. This implies that the Variscan orogeny resulted in geochemically and isotopically heterogeneous lithospheric mantle on the regional scale, possibly reflecting the contrasting nature of the subducted rocks.

1. Introduction

Calc-alkaline lamprophyres are hypabyssal rocks that commonly form dikes and sills and that are characterized by a panidiomorphic porphyritic texture with abundant phenocrysts of amphibole and/or dark mica. Lamprophyres are widely considered to be primary mantle-derived magmas (e.g., Rock, 1991; Bédard, 1994) that provide not only important information for magma genesis in the mantle, but also on geodynamic processes modifying the mantle and leading to the extraction of lamprophyric melts. Although lamprophyres were long thought to sample a metasomatized mantle source, which may have been enriched during an ancient event, it has become increasingly obvious that the trace-element and isotopic signatures of old crust-derived material may well equally have been introduced during geologically young events (e.g., Hegner et al., 1998; Hoch et al., 2001; Prelević et al., 2005, 2012). The geochemical composition of lamprophyres shows an uncoupling of the major and compatible trace element contents (i.e., high MgO, Cr, and Ni) and high Mg# values, which reflect the mantle source, from the incompatible trace element and rare earth element contents and the isotope composition of Sr, Nd, and Pb, which typically reflect a crustal source. In previous studies, this geochemical uncoupling in lamprophyric magma has been variably linked to a low degree of partial melting of lithospheric mantle peridotites, metasomatized mantle sources in a subduction setting, mixing of mantle and crustal melts, and assimilation with fractional crystallization (e.g., Jones and Smith, 1983; Macdonald et al., 1985; Turpin et al., 1988; Stille et al., 1989; Rock, 1991; Currie and Williams, 1993; Prelević et al., 2004, 2007; Janoušek et al., 2010). Prelević et al. (2005, 2010) noticed a close correspondence between the geochemical and isotopic signature of Mediterranean orogenic lamproites and the sediments in the trench and the sedimentary wedge. This indicates that the local geochemical signature of the material entering into the subduction zone resurfaces in the orogenic lamproites extracted from the mantle above the subducting plate (Prelević et al., 2005). This correspondence not only demonstrates that metasomatism of the mantle in the orogenic lamproite (and more generally in the lamprophyre) source may occur shortly before they are extracted, but also opens the possibility to use orogenic lamproites and lamprophyres to trace the composition of subducting plate in young and ancient orogens. The geochemical signature of orogenic lamproites and possibly also calc-alkaline lamprophyres

* Corresponding author.
E-mail address: khaled@gfz-potsdam.de (K.M. Abdelfadil).

0009-2541/$ – see front matter © 2012 Elsevier B.V. All rights reserved.
http://dx.doi.org/10.1016/j.chemgeo.2012.10.023

may be used to trace post-collisional interaction between an orogenic lithospheric mantle and a shallow subducting plate (cf. Prelević et al., 2010).

The Variscan orogen resulted from the collision of Laurussia with Gondwana and several smaller crustal blocks (i.e., Bohemia, Brittany, Iberia) between them. These crustal blocks, dominated by Cadomian basement (c. 570 to 545 Ma), are bordered by belts of Variscan high-grade metamorphic rocks (e.g., Erzgebirge, Sudetes, Vosges, Black Forest) that are interpreted to trace belts of Variscan subduction zones (e.g., Matte, 1991; Franke, 2000; Matte, 2001). The scarcity of subduction-related magmatism indicates that along these zones predominantly thinned continental crust – and its sedimentary cover – was subducted. These rocks are now largely preserved in Variscan high-grade metamorphic rocks. Post-collisional magmatism includes voluminous syn- and post-tectonic granitoids that are mostly derived from crustal melting (e.g., Turpin et al., 1990; Finger et al., 1997; Förster and Romer, 2010). Subduction of thinned continental crust and its sedimentary cover resulted in the metasomatism of the mantle above the subducted plate. This metasomatized mantle was sampled by a suite of late-orogenic lamprophyre dikes, most importantly among them calc-alkaline lamprophyres (Turpin et al., 1988; Wenzel et al., 1991; Hegner et al., 1998; von Seckendorff et al., 2004; Awdankiewicz, 2007; Seifert, 2008). In analogy to the geochemical variability of the Mediterranean orogenic lamproites that reflect the regional variability of the subducted sediments, the regional distribution of calc-alkaline lamprophyres may reflect the distribution of Variscan subduction zones and the regional geochemical variation among these lamprophyres may trace the contrasting character of the subducted material.

Lusatia is one of these Cadomian blocks that largely escaped Variscan metamorphism and deformation and that differs from adjacent parts of the Bohemian Massif by the absence of piles of Variscan high-grade metamorphic rocks. The Cadomian basement of Lusatia (greywackes and granodiorites; Fig. 1) has been intruded by pre-Variscan gabbros and by late-Variscan lamprophyres. The compositional variations between the pre-Variscan gabbros and late-Variscan lamprophyres allow us to characterize the effect of material subducted during the Variscan orogeny on the mantle beneath Lusatia. Furthermore, the contrasting Variscan development of Lusatia and adjacent regions with Variscan high-grade metamorphic rocks may find its expression in contrasting metasomatism of the mantle source for the lamprophyric magmatism. In this paper, we present mineralogical, geochemical, and Sr, Nd, and Pb isotope data of pre-Variscan gabbros and late-Variscan calc-alkaline lamprophyres to characterize the geochemical and isotopic effect of the Variscan (and possibly Cadomian) orogeny on the mantle beneath Lusatia.

2. Geological setting

The Cambrian to Ordovician rifting of the northern margin of Gondwana, which eventually led to the opening of the Rheic Ocean, resulted in the formation of two types of continental crust, i.e., blocks with continental crust of normal thickness that are separated by thinned continental crust that developed into shelf areas with marine sedimentation (e.g., Linnemann et al., 2000; Kroner et al., 2007; Linnemann et al., 2008; Heuse et al., 2010; Kroner and Romer, 2010; Linnemann et al., 2010a). The blocks of normal crustal thickness are dominated by metamorphic and voluminous magmatic rocks of the former Cadomian magmatic arc (570 to 545 Ma, Linnemann et al., 2000, 2008). The areas of thinned continental crust developed into sedimentation areas that record the successive development of rift-bound sedimentation with siliciclastic debris from the Cadomian arc to shallow and eventually to deep shelf sedimentation (Linnemann et al., 2004, 2010b). During the Variscan orogeny, these blocks of thick Cadomian continental crust and the zones of thinned continental crust behaved differently: The areas of thick crust were not subductible, whereas the areas of thin continental crust were subductible (cf. Kroner et al., 2007; Kroner and Romer, 2010). The closure of the Rheic Ocean initially was accomplished by consumption of oceanic crust beneath the Mid-German Crystalline Zone, eventually leading to the docking of Gondwana-derived blocks to Laurussia. Once a block of thick Cadomian continental crust had docked to Laurussia, a new subduction zone was initiated behind this block. In these later subduction zones, thinned continental crust and its sedimentary cover was subducted until the next block of thick Cadomian continental crust arrived and collided, resulting in the generation of yet another subduction zone. With the arrest of subduction, the subducted continental crust escaped from beneath the blocks of thick Cadomian continental crust – either by lateral escape or backflow in the subduction channel – and was emplaced as stacks of nappes of contrasting metamorphic history on adjacent terranes (cf. Kroner et al., 2007, 2010; Kroner and Romer, 2010). Subduction of thinned continental crust and formation of new subduction zones behind blocks of thick crust (i) explains the occurrence of high grade metamorphic rocks in close spatial association with areas of little Variscan overprint, (ii) accounts for the scarcity of subduction-related Variscan magmatism, and (iii) brings thinned continental crust and its sedimentary cover to mantle depth (e.g., Kroner et al., 2007, 2008; Kroner and Romer, 2010). Fluid-loss from these sediments and possible partial melting of the sediments and their crystalline substratum provides the agents that may metasomatize the mantle above the subducting plate.

The Bohemian Massif and in particular the Lusatian block are special as they are among the first Gondwana-derived blocks to collide with Laurussia. The approach of Bohemia and Laurussia resulted in the thrusting of the Tepla-Barrandian Unit onto other parts of the Bohemian Massif, the formation of the Sudetes, and in establishing a new subduction zone to the SW of the Bohemian Massif. Lusatia was at that time not a part of the Bohemian Massif and continued to move toward Laurussia. The strike slip zone between Bohemia and Lusatia later was reactivated during the subsequent lateral escape of subducted crustal rocks from beneath Bohemia and their emplacement onto the Saxo-Thuringian Zone to form the Erzgebirge (cf. Kroner et al., 2007, 2010; Kroner and Goerz, 2010; Kroner and Romer, 2010).

Lusatia, located at the northeastern margin of the Bohemian Massif, is bordered to the SW by the Elbe-Fault Zone and to the NE by faults paralleling the Görlitz slate belt (Fig. 1). These structural elements have been active during the Variscan orogeny and have been repeatedly reactivated since. To the south, Lusatia is bordered by the Tertiary Eger rift, which largely follows the strike slip zone along which Lusatia had slipped by the Bohemian Massif during the Variscan orogeny. To the north Lusatia is separated from the Mid-German Crystalline Zone by a major shear zone. In the southern part of Lusatia, where Cadomian granodiorites predominate, several stocks and dike swarms of gabbroic rocks, in particular gabbro norite, olivine gabbro, and diorite (Kramer et al., 1977), had intruded. Kramer et al. (1977) reported a K–Ar whole rock age of 400 Ma for the gabbros in Lusatia. This age later was confirmed by a Pb–Pb age of 390 ± 8 Ma (zircon evaporation; Kindermann et al., 2003) for a gabbro near Valtengrund (Fig. 1). The gabbros have been emplaced in stable crust and show within-plate geochemical signatures (e.g., Peschel et al., 1973; Kramer, 1988; Heinrich, 1993). The occurrence of gabbroic rocks of this age and setting in Lusatia is unusual: in other parts of the Saxo-Thuringian Zone, gabbros are much older and related to the opening of the Rheic Ocean (e.g., Vesser Zone, Kemnitz et al., 2002; Münchberg, Stosch and Lugmair, 1990). In the West-Sudetes (i.e., at Braszowice and Sleza) occur gabbros of corresponding age, i.e., 400 ± 10 Ma (Kryza and Pin, 2010) and 420 ± 20 Ma (Oliver et al., 1993), but there, the gabbros are part of ophiolitic successions (Kryza and Pin, 2010).

The Cadomian granodiorites and greywackes and the pre-Variscan gabbros of Lusatia are intruded by (i) dike swarms of alkaline basalt with unknown – but pre-Variscan – age (Kramer, 1988) and (ii) late-Variscan dikes of older calc-alkaline lamprophyres (this study), and 315–304 Ma old post-Variscan granite intrusions (Eidam et al., 1995; Fig. 1), as well as post-Variscan dike swarms of (iii) andesites, rhyodacites,

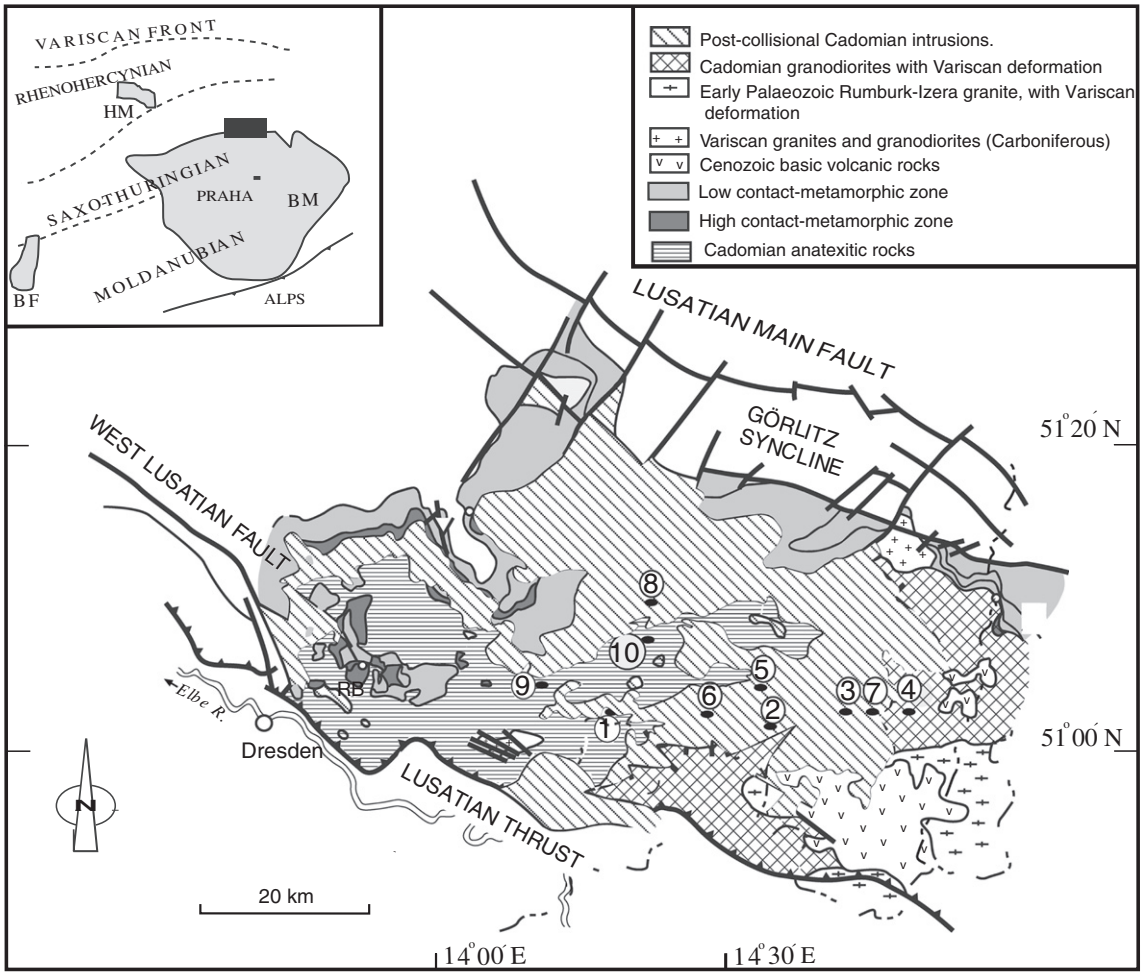

Fig. 1. Geological map of the Lusatian Block in the Saxo-Thuringian Domain. Sampling locations: 1—Valtengrund (51°04' N, 14°17′ E), 2—Klunst Ebersbach (51°01′ N, 14°35′ E), 3—Das Gericht (51°02′ N, 14°41′ E), 4—Julienstein (51°02′ N, 14°44′ E), 5—Israel (51°04′ N, 14°32′ E), 6—Hutzelberg (51°02′ N, 14°32′ E), 7—Strahwalde (51°02′ N, 14°43′ E), 8—Bautzen-Stiebitz (51°10′ N, 14°23′ E), 9—Fichtenberg (51°05′ N, 14°13′ E), 10—Soraer Höhe (51°08′ N, 14°22′ E). The gabbro samples were collected at locations 1, 2, 8, 9, and 10, whereas the lamprophyres at 3, 4, 5, 6, and 7. Post-collisional Cadomian intrusions occur as plutons and are granodioritic in composition. Inset shows the position of Lusatia relative to major Variscan massifs and zones. BM: Bohemian Massif; BF: Black Forest; HM; Harz Mountains.
Geological map is after Kemnitz (2007).

rhyolite, and younger lamprophyres (Eidam et al., 2001). The calc-alkaline lamprophyres are spessartites (amphibole and plagioclase dominant). They form NE to SW trending dikes that may reach a 25 m width (Kramer et al., 1977). The age of these dikes is not well known and the K/Ar age of 230 Ma (Kramer et al., 1977) is inconsistent with the emplacement age of lamprophyres from other parts of Variscan Europe, e.g., the Sudetes, the Black Forest, the Erzgebirge, and the French Massif Central (Turpin et al., 1988; Hegner et al., 1998; Awdankiewicz, 2007; Seifert, 2008), all of which have been emplaced during the late stages of the Variscan orogeny.

The Palaeozoic (post-Cadomian and pre-Variscan) tholeiitic gabbros and the late-Variscan calc-alkaline lamprophyres (spessartite) sampled the mantle beneath Lusatia, which allows to characterize the effect of the Variscan orogeny on the mantle and to compare it with the metasomatized mantle beneath the Erzgebirge and the Sudetes. As the latter areas have been much more intensely involved into the Variscan orogeny, they may have a different extent and/or signature of mantle metasomatism.

3. Samples and analytical methods

We present data from eleven gabbro samples and eleven relatively fresh calc-alkaline lamprophyres collected from Lusatia. The gabbro samples were collected at five locations (Valtengrund, Fichtenberg, Soraer Höhe, Bautzen-Stiebitz, and Klunst Ebersbach, Fig. 1) and the calc-alkaline lamprophyres were sampled from small dikes at five locations (Israel, Hutzelberg, Strahwalde, Julienstein, and Das Gericht, Fig. 1). As the age of the lamprophyres was known only from K–Ar whole-rock dating, we separated amphibole from two spessartite samples collected at Das Gericht and Julienstein for Ar/Ar dating.

Amphibole Ar–Ar dating was performed at the geochronology laboratory of the University of Potsdam. Amphibole was separated from the 250 to 200 μm fraction and purified by hand-picking under a binocular microscope. The samples were irradiated at the Geesthacht Neutron Facility (GeNF), GKSS Research Center, Germany, for 96 h with a fast neutron flux of 1×1012 n/cm^2/s. As monitors for the neutron flux and the production of Ar from Ca and K, we used Fish Canyon tuff sanidine and crystals of CaF_2 and K_2SO_4, respectively. For the Fish Canyon tuff sanidine, we used an age of 27.5 Ma (Uto et al., 1997; Ishizuka, 1998; Ishizuka et al., 2002), which agrees with the one obtained by Lanphere and Baadsgaard (2001). The samples were analyzed by stepwise heating until total fusion, using a 50 W CO_2 laser operated at a wavelength of 10.6 μm involved in the Dual Wave laser ablation system. The extracted gas was purified using cold traps and Zr–Al SEALS alloy getters and analyzed using a Micromass 5400 noble gas mass spectrometer with high sensitivity and low background. System blanks were measured after every three samples. The measured isotopic ratios were corrected for blank measurements, mass discrimination, interference of Ar isotopes

Table 1
$^{40}Ar/^{39}Ar$ step-heating data for amphiboles from calc-alkaline lamprophyre, Lusatia, Germany.

Laser output	$^{40}Ar/^{39}Ar$	$^{37}Ar/^{39}Ar$	$^{36}Ar/^{39}Ar$ (×10−3)	K/Ca	$^{40}Ar^*$ (%)	$^{39}Ar_K$ fraction (%)	$^{40}Ar^*/^{39}Ar_K$	Age (±1 s) (Ma)
Sample 2680, Das Gericht, J = 0.00149								
0.018	923 ± 10	54.2 ± 128.7	682.3 ± 2.8	0.01	78.89	0.31	766 ± 96	1374 ± 120
0.02	239.2 ± 1.7	238 ± 174	191 ± 7	0.00	88.80	0.18	271 ± 61	612 ± 117
0.024	230.3 ± 0.9	99 ± 83	175 ± 3	0.01	82.90	0.45	210 ± 21	491 ± 42
0.028	140.4 ± 0.9	48 ± 36	54.1 ± 1.4	0.01	92.88	1.03	136 ± 7	334 ± 15
0.032	146.6 ± 0.4	1 ± 7	21.6 ± 0.4	1.02	95.69	5.10	140.3 ± 1.4	343 ± 3
0.034	133.8 ± 0.3	6 ± 3	10.30 ± 0.12	0.09	98.31	11.91	132.3 ± 0.6	324.9 ± 1.7
0.035	130.9 ± 0.3	33 ± 5	10.84 ± 0.20	0.02	99.48	19.08	134.1 ± 1.0	329 ± 2
0.036	128.5 ± 0.2	32 ± 5	8.3 ± 0.2	0.02	99.37	15.82	131.4 ± 0.9	323 ± 2
0.038	126.7 ± 0.8	14.6 ± 1.9	8.14 ± 0.09	0.04	99.53	46.13	127.8 ± 0.9	315 ± 2
Sample 2693, Julienstein, J = 0.00149,								
0.02	573.1 ± 2.9	131 ± 52	693 ± 9	0.00	67.10	0.70	436 ± 25	903 ± 40
0.025	198.2 ± 1.6	139 ± 44	308 ± 3	0.00	62.83	0.87	142 ± 9	347 ± 20
0.028	149.6 ± 0.5	73 ± 22	50.4 ± 1.0	0.01	96.08	1.76	154 ± 4	373 ± 10
0.03	135.5 ± 0.6	37 ± 10	23.0 ± 0.5	0.02	98.41	4.24	138.0 ± 2.0	338 ± 5
0.032	140.3 ± 0.3	1 ± 3	12.92 ± 0.12	0.75	97.35	12.92	136.7 ± 0.7	334.6 ± 1.9
0.034	136.0 ± 0.6	36 ± 6	9.49 ± 0.17	0.02	99.41	19.37	139.7 ± 1.3	341 ± 3
0.036	134.6 ± 0.5	15 ± 3	7.15 ± 0.13	0.04	99.79	50.89	136.1 ± 0.7	333 ± 2
0.037	128.97 ± 0.06	4 ± 5	5.2 ± 0.2	0.13	99.22	9.25	128.5 ± 0.9	316 ± 2

derived from Ca and K by irradiation, and post irradiation decay of ^{37}Ar and ^{39}Ar. The final age calculation and errors follow the procedure of Uto et al. (1997). The following three criteria were used to define a plateau for the dated samples; (1) the plateau has to include a series of adjacent steps that together comprise more than 50% of the released ^{39}Ar, (2) the ages of the steps should agree within two sigma (2σ) error, (3) each degassing step included in the plateau should have more than 3% of the total ^{39}Ar released.

Mineral analyses were performed using a CAMECA SX100 electron microprobe operated at 15 kV accelerating voltage, a beam current of 20 nA, and a variable beam diameter of 1 to 15 μm. Peak counting times were 10–20 s for major and 30 s for minor elements; backgrounds were counted for 5–15 s. Data reduction used the PAP correction procedure implemented in the CAMECA software.

Major and trace element analyses were carried out at Deutsches GeoForschungZentrum (GFZ). Major element oxides and the trace elements Ba, Cr, Ga, Nb, Ni, Rb, Sr, V, Y, Zn, and Zr were analyzed by XRF on fused disks prepared from dried (105 °C) powders (<60 μm) and Li tetraborate–metaborate (Fluxana FX-X65) at a sample-to-flux ratio of 1:6. Concentrations were determined using a Panalytical Axios advanced wavelength-dispersive spectrometer and matrix correction programs. H_2O+ and CO_2 were determined using a Vario EL III using high-temperature catalytic combustion. Trace elements (Nb, Mo, Cd, Cs, Ti, Pb, Th, U, Sc, Co, Cu, Ga, Sb, and Sn) were determined by IC-MS using a VG Plasma Quad PG2. Sample powders were decomposed using HF, Aqua regia, and $HClO_4$. The dissolved samples were redissolved in HNO_3 and diluted to a volume of 50 ml for analysis. Rare earth element (REE) and Y contents were determined by inductively coupled plasma-atomic emission spectroscopy (ICP-AES) following the procedure of Zuleger and Erzinger (1988). The samples are decomposed using Na_2O_2 and the REE are separated and concentrated chromatographically using ion-exchange methods.

Whole-rock Nd, Sr, and Pb isotopic compositions were analyzed at Deutsches GeoForschungZentrum. Samples were dissolved using

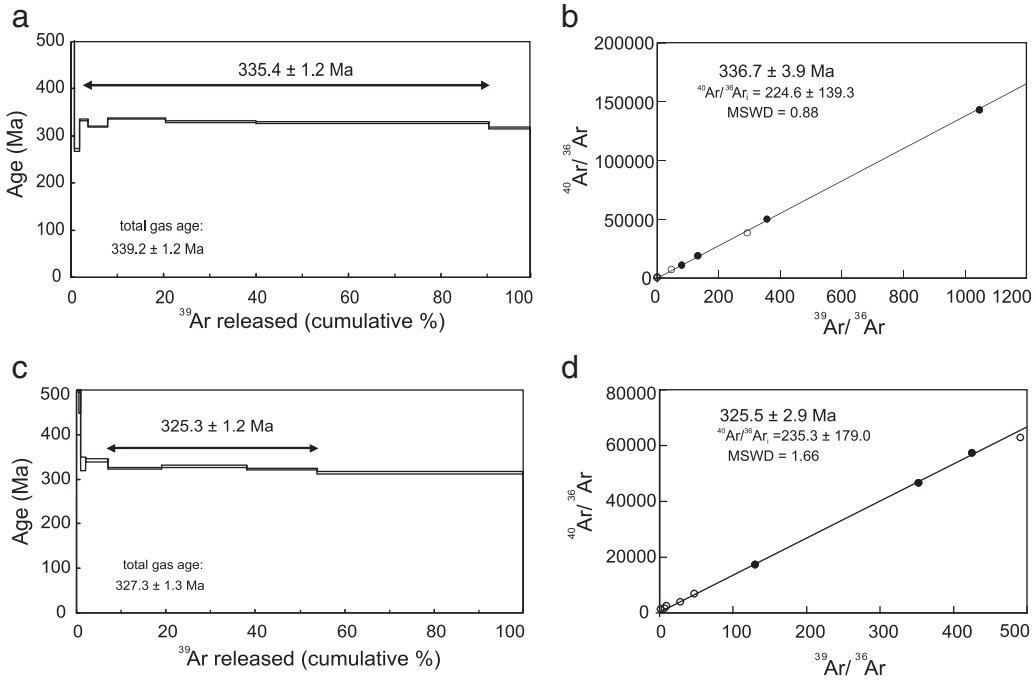

Fig. 2. $^{40}Ar/^{39}Ar$ age spectra (left) and isotope correlation diagrams (right) for the hornblende samples of two lamprophyres from Lusatia. MSWD—mean square of the weighted deviates. Filled symbols are the data of the "plateau steps" in the "age spectrum". Open symbols are the data of the other steps in the "age spectrum".

Table 2
Representative electron microprobe analyses of clinopyroxene, amphibole, and plagioclase from calc-alkaline lamprophyre and gabbros.

	Clinopyroxene								Amphibole								Feldspar				
	Spessartites				Gabbros				Spessartites				Gabbros				Spessartites			Gabbros	
									TMH	TMH	Ka	TPg	M Hb	TM Hb	FM Hb	M Hb	Kfs	Pl	Pl	Pl	Pl
Sample	S16c	S16r	S17c	S17r	S23c	S23r	S9c	S9r	101Dr	101Dc	S17c	S17r	S13c	S13	S13c	S13r	S12	S12c	S12r	S0p8c	S9p8r
SiO_2	50.43	50.76	51.78	51.62	52.52	52.49	51.48	52.24	41.74	41.71	41.64	42.09	48.92	47.65	48.73	48.24	63.92	66.34	66.11	55.64	56.74
TiO_2	0.77	0.71	0.60	0.55	0.66	0.58	0.79	0.69	4.50	4.44	4.49	4.40	1.27	2.48	1.24	1.29	na	na	na	na	na
Al_2O_3	3.21	3.26	2.20	2.32	2.66	2.19	2.73	2.58	11.47	11.36	11.36	11.37	5.43	3.95	5.37	5.74	18.22	20.67	21.01	27.26	26.84
Cr_2O_3	0.18	0.30	0.21	0.30	0.001	0.001	0.001	0.001	0.03	0.00	0.00	0.01	0.03	0.02	0.03	0.02	na	na	na	na	na
MgO	15.62	15.90	16.66	16.74	16.18	17.22	15.52	15.56	13.06	13.04	12.98	12.87	11.21	11.33	12.06	11.33	0.00	0.01	0.00	0.11	0.08
CaO	20.18	19.90	19.02	19.13	17.54	15.18	17.56	17.75	11.65	11.55	11.50	11.64	11.12	13.12	9.97	10.97	0.06	1.76	2.08	10.54	9.71
MnO	0.20	0.21	0.22	0.23	0.30	0.30	0.25	0.25	0.19	0.21	0.15	0.18	0.21	0.35	0.28	0.20	0.02	0.00	0.01	0.02	0.00
FeO	8.05	7.95	8.79	8.04	10.38	12.48	11.20	10.48	11.78	11.94	11.31	12.19	18.15	17.47	18.24	17.20	0.05	0.02	0.16	0.63	0.53
Na_2O	0.37	0.33	0.27	0.30	0.35	0.28	0.36	0.37	2.25	2.42	2.32	2.44	1.02	0.68	1.11	1.04	0.37	10.88	10.98	5.55	6.00
K_2O	0.01	0.00	0.00	0.00	0.01	0.00	0.01	0.00	1.07	1.11	1.09	1.06	0.45	0.55	0.50	0.52	15.31	0.08	0.06	0.28	0.35
Total	99.02	99.31	99.74	99.23	100.6	100.7	99.91	99.92	97.78	97.80	96.86	98.2	97.84	97.20	97.57	96.58	99.05	99.75	100.4	100	100.3
Si	1.89	1.89	1.92	1.92	1.93	1.94	1.92	1.94	6.16	6.16	6.198	6.195	7.20	7.167	7.08	7.174	2.995	2.920	2.899	2.515	2.551
Ti	0.02	0.02	0.02	0.02	0.02	0.02	0.02	0.02	0.50	0.49	0.503	0.487	0.14	0.281	0.14	0.144	na	na	na	na	na
Al	0.14	0.14	0.10	0.10	0.12	0.10	0.12	0.11									1.006	1.072	1.086	1.452	1.422
Mg	0.87	0.88	0.92	0.93	0.89	0.95	0.86	0.86	2.87	2.87	2.879	2.823	2.46	2.540	2.61	2.512	0.000	0.001	0.000	0.007	0.005
Ca	0.81	0.80	0.76	0.76	0.69	0.60	0.70	0.71	1.84	1.83	1.835	1.835	1.75	2.115	1.55	1.748	0.003	0.083	0.098	0.511	0.468
Mn	0.01	0.01	0.01	0.01	0.01	0.01	0.01	0.01	0.02	0.03	0.019	0.022	0.03	0.045	0.03	0.025	0.001	0.000	0.001	0.001	0.000
Fe^2	0.25	0.25	0.27	0.25	0.32	0.39	0.35	0.33	1.29	1.31	1.347	.401	1.73	2.197	1.08	1.675	0.002	0.001	0.006	0.024	0.020
Na	0.03	0.02	0.02	0.02	0.03	0.02	0.03	0.03	0.64	0.69	0.668	0.695	0.29	0.199	0.31	0.300	0.033	0.928	0.934	0.486	0.523
Al^{IV}	0.11	0.11	0.08	0.08	0.07	0.06	0.08	0.06	1.84	1.84	1.802	1.805	0.80	0.701	0.920	0.826					
Al^{VI}	0.03	0.04	0.02	0.02	0.05	0.03	0.04	0.05	0.15	0.14	0.190	0.167	0.14	0.000	0.00	0.180					
Wo	40.01	38.72	37.51	37.63	33.40	29.40	34.36	34.00													
En	46.55	47.85	48.22	49.13	48.98	50.19	46.73	47.90													
Fs	13.45	13.42	14.27	13.24	17.62	20.41	18.91	18.10													
Mg#	78	78	77	79	74	71	71	73	69	68	681	66	59	53	71	60					

Cation calculated on the basis of 6 O for pyroxene, 23 for amphibole, and 8 for feldspar. Kfs: K. Feldspar, Pl: plagioclase, na: not analyzed. Mg#: $100*Mg/(Mg+Fe^{+2})$, Wo: wollastonite; En: enstatite; Fs: ferrosilite; M Hb: magnesio-hornblende; FM Hb: ferri-magnesio-hornblende; TM Hb: titanian magnesio-hornblende; TMH: titanian magnesiohastingsite; ka: kaersutite; TPg: titanian pargasite.

concentrated HF for four days at 160 °C on a hotplate. To transfer fluorides into nitrates, the digested samples were dried and taken up in HNO_3 and dried again. Hereafter, the samples were re-dissolved in 6 N HCl and splitted for Pb and Sr–Nd ion-chromatographic separation. Pb was separated using the HCl-HBr ion exchange chemistry described by Romer et al. (2005). Pb was loaded together with H_3PO_4 and silica-gel on single Re-filaments and its isotopic composition was measured at temperatures between 1200 and 1250 °C on a Finnigan MAT262 TIMS multi-collector mass spectrometer using static multicollection. Instrumental mass-fractionation was corrected using 0.1% per a.m.u. as determined from the repeated measurement of the NBS SRM 981 standard. Accuracy and precision of the Pb isotopic ratio is better than 0.1% at the 2σ level. Total procedural blanks are better than 15–30 pg Pb. Sr and Nd were separated using cation-exchange chromatographic procedures. The Sr and Nd isotopic composition was determined on a Triton and a Finnigan MAT262 multi-collector mass-spectrometer, respectively, operated in dynamic multicollection mode. $^{87}Sr/^{86}Sr$ and $^{143}Nd/^{144}Nd$ were normalized to $^{86}Sr/^{88}Sr = 0.1194$ and Nd $^{146}Nd/^{144}Nd = 0.7219$, respectively. During the period of analytical work the Sr reference material NBS987 gave $^{87}Sr/^{86}Sr = 0.710249 \pm 0.000005$ (n = 20) and the La Jolla Nd reference material gave $^{143}Nd/^{144}Nd = 0.511855 \pm 0.000006$ (n = 14). Total procedural blanks for Sr and Nd analyses are less than 50 pg Sr and less than 30 pg Nd.

4. Results

4.1. ^{40}Ar–^{39}Ar age dating of lamprophyres

The ^{40}Ar–^{39}Ar data are presented in Table 1 and Fig. 2. The Ar-release spectrum of hornblende from Julienstein (sample 2693) yields a plateau that is defined by five steps and more than 80% of ^{39}Ar-release. The low-temperature Ar-release, which encompasses only 3% of the spectrum and yields anomalously old apparent ages, and the last high-temperature step, which yields a slightly lower age than the plateau, have been excluded. The plateau corresponds to a ^{39}Ar–^{40}Ar age of 335.4 ± 1.2 Ma (Fig. 2a), which is within uncertainties identical with the 336.7 ± 3.9 Ma obtained from the $^{40}Ar/^{36}Ar$ vs. $^{39}Ar/^{46}Ar$ isochron with a mean square of weighted deviations (MSWD) of 0.88 (Fig. 2b). This total gas age of 339.2 ± 1.2 Ma is slightly older, reflecting the contribution of the small, but highly anomalous first release step.

The Ar-release spectrum of hornblende from the lamprophyre of the location Das Gericht (sample 2683) yields a three-step plateau age that includes 53.2% of the released ^{39}Ar. This plateau age corresponds to an age of 325.3 ± 1.2 Ma (Fig. 2c), which agrees within uncertainties with the 325.5 ± 2.9 Ma obtained for the isochron (MSWD = 1.66; Fig. 2d). Note, both amphibole samples yield initial $^{40}Ar/^{36}Ar$ values that are within uncertainties identical with the Ar composition of air, i.e., there seems to be no excess argon except for the low-temperature degassing steps.

The plateau ages of 325.3 ± 1.2 Ma and 335.4 ± 1.2 Ma for hornblende from the two spessartite samples are considered to date the time of lamprophyre emplacement. Our new ^{39}Ar–^{40}Ar ages are markedly older than the whole-rock K/Ar age of c. 230 Ma and supersede this age. The new ages show that the lamprophyres were emplaced during the late stage of the Variscan orogeny. The new age data imply that lamprophyric magmatism in Lusatia is coeval not only with lamprophyre emplacement in the adjacent areas of the Erzgebirge, the Sudetes, and the Moldanubian Zone of the Bohemian Massif (von Seckendorff et al., 2004; Awdankiewicz, 2007; Janoušek and Holub, 2007; Seifert, 2008), but also with lamprophyres from other parts of the Variscan orogen, such as the Black Forest, the Vosges, the French Massif Central, and the Balkan range (Turpin et al., 1988; Hegner et al., 1998; Buzzi et al., 2010).

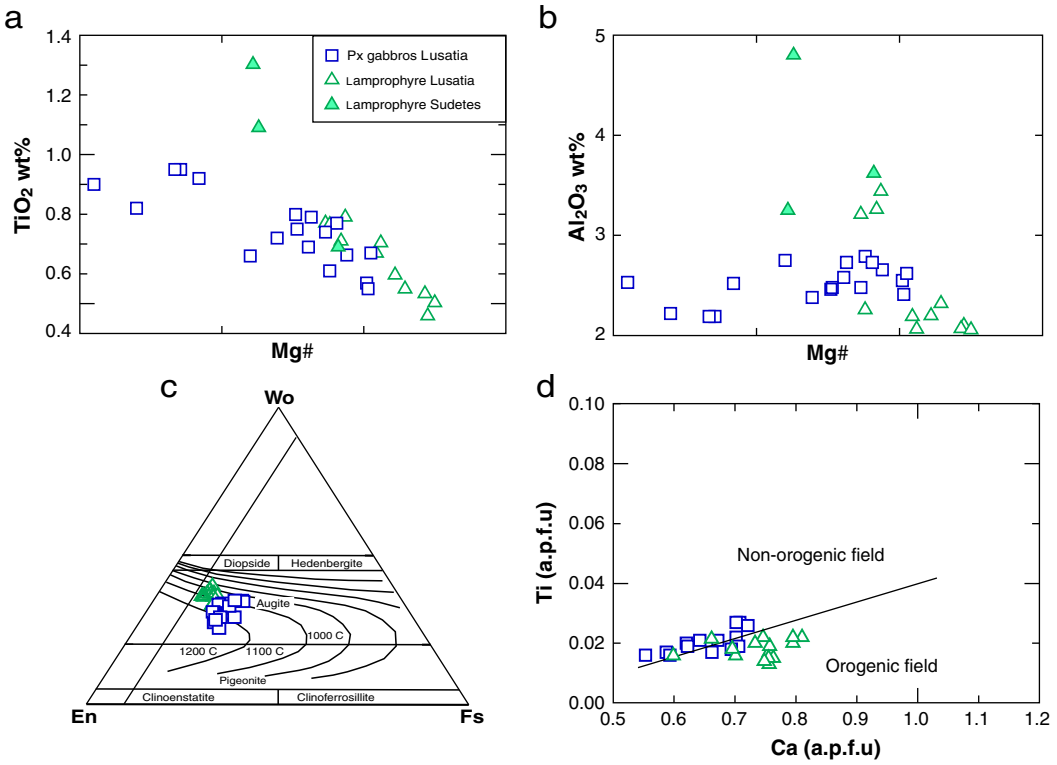

Fig. 3. a) Mg# vs. TiO_2; b) Mg# vs. Al_2O_3; c) Cpx triplot after Morimoto (1988), pyroxene thermometry after Lindsley (1983); d) Ca vs. Ti binary diagrams after Letterrier et al. (1982) modified by Sun and Bertrand (1991). a.p.f.u.—atoms per formula unit. Clinopyroxene composition from the Sudetes after Awdankiewicz (2007).

4.2. Petrographic description

4.2.1. Gabbros

Post-Cadomian and pre-Variscan intrusions in Lusatia form major bodies dominated by gabbro and olivine gabbro with local domains (at the decimeter to meter scale) of pegmatitic gabbro. The gabbro is mainly composed of clinopyroxene (c.40 vol.%), plagioclase (c.54 vol.%), and minor amounts of hornblende and biotite. Secondary minerals are actinolite, chlorite, epidote, zoisite, and sericite. Plagioclase forms subhedral labradorite to andesine crystals (Table 2). It is occasionally altered to sericite, epidote, and zoisite. Augite is partly replaced by chlorite. Ophitic and subophitic textures are common. The olivine gabbro, which is dominated by clinopyroxene (augite), plagioclase, and amphibole, in addition has pseudomorph serpentine after olivine. Pegmatitic gabbro is composed mainly of very coarse grained plagioclase and clinopyroxene with minor amounts of biotite. Chlorite is the main secondary mineral and apatite is the main accessory mineral. Quartz is interstitial. Some pyroxene is altered to iron oxide and chlorite. There are two generations of biotite, a primary yellow to dark brown pleochroic one and a secondary one after pyroxene. Locally, biotite is rimmed by chlorite and iron oxide.

Amphibole is calcic (Table 2) and ranges according to the classification of Hawthorne and Oberti (2007) from titanian magnesio-hornblende, ferrian magnesio-hornblende, actinolitic hornblende to magnesio-hornblende. The end-member composition for clinopyroxene from the gabbros is $En_{39–52}Wo_{26–40}Fs_{17–24}$ (Table 2).

4.2.2. Calc-alkaline lamprophyres

Spessartite from Lusatia has a porphyritic to panidiomorphic texture, dominantly euhedral amphibole (c.38 vol.%) and more rarely clinopyroxene phenocrysts, and a groundmass of plagioclase (c.40 vol.%), minor amounts of intergrown K-feldspar and quartz, and accessory apatite and titanite. Amphibole is strongly pleochroic (brown to dark brown) and ranges from titanian magnesiohastingsite to pargasite and kaersutite (Table 2) (Kramer, 1976, 1988; Kramer and Andrehs, 2011). Amphibole is zoned with Si and Fe increasing and Al, Cr, Na, and F decreasing from core to rim. Along the rims, amphibole may show overgrowth of actinolite with $X_{Mg} = 0.66$ (Table 2) and along cracks it may be replaced by chlorite and epidote. Plagioclase is a common groundmass component, forms only rarely phenocrysts, and is typically strongly sericitized and albitized. It is albite and has the composition $Kfs_{0.8}Ab_{91}An_{8.2}$ (Table 2). The clinopyroxene composition in calc-alkaline lamprophyre from Lusatia is similar to the one of clinopyroxene in spessartite from the Sudetes (Fig. 3), but differs from the one of clinopyroxene from Lusatian gabbros, which have lower CaO, Cr_2O_3 and Mg# and higher MnO, Na_2O, SiO_2, TiO_2, and FeO (Table 2). It is Ca rich augite ($Wo_{36–40}En_{46–50.9}Fs_{12–16}$; Table 2; Fig. 3c) and rarely forms phenocrysts. According to Lindsley (1983), the clinopyroxene composition indicates crystallization temperatures that range from 900 °C to ~1200 °C for the calc-alkaline lamprophyre and from 1000 °C to ~1200 °C for the gabbros (Fig. 3c). Clinopyroxene from the gabbros and calc-alkaline lamprophyres have similar Ti/Al ratios (between 0.25 and 0.125). On the Ca–Ti discrimination diagram, clinopyroxene of the calc-alkaline lamprophyre mostly plot in the orogenic field consistent with formation in a subduction-related tectonic setting. The tholeiitic gabbro pyroxenes plot along the line separating the orogenic and non-orogenic fields (Fig. 3d).

4.3. Whole rock geochemistry of investigated rocks

Chemical analyses of 21 representative samples of the gabbros and spessartites are given in Table 3. Chemical variations among them are shown in Harker diagrams (Fig. 4). In the Alk–FeO*–MgO diagram of Irvine and Baragar (1971) (not shown), the gabbros are tholeiitic and the lamprophyres show a calc-alkaline trend. The lamprophyre samples fall within the range of calc-alkaline lamprophyres following the classification of Rock (1977 and 1991). In the total alkali silica (TAS) diagram

Table 3
Geochemical data of gabbros and calc-alkaline lamprophyres from Lusatia.

Rock	Gabbro											Calc-alkaline lamprophyre									
	gb	gb	pg-gb	pg-gb	ol-gb	ol-gb	dt	ol-gb	gb	gb	gb-nt	sp.	sp.	sp.	sp.	sp.	sp.	sp.	sp.	sp.	sp.
No	VG1	VG2	VG3	VG4	KE5	KE6	BS7	VG8	SH9	FB10	SH11	DG12	DG13	JS14	JS15	JS16	DG17	JS18	SW19	HB20	IS21
SiO_2	48.9	49.0	49.0	48.9	46.5	47.7	48.8	50.3	48.4	49.4	47.9	51.1	49.9	48.6	48.7	46.5	50.5	52.1	51.7	53.7	53.0
TiO_2	1.43	1.35	1.22	1.34	1.18	1.10	2.05	1.16	1.16	1.03	1.28	1.54	1.53	1.33	1.32	2.46	1.92	1.38	1.73	1.08	1.61
Al_2O_3	16.3	16.6	16.6	16.5	16.9	17.9	15.5	16.3	18.3	12.4	13.4	16.3	15.9	14.5	14.4	14.4	15.4	16.6	14.3	15.8	16.9
FeOt	10.5	10.8	10.6	10.8	9.2	8.8	13	10.5	9	10.6	11.5	8.3	8.3	10.1	10.1	9.4	9	7.3	8.7	5.9	9.8
MnO	0.16	0.16	0.16	0.16	0.15	0.14	0.15	0.14	0.13	0.15	0.16	0.15	0.15	0.16	0.16	0.17	0.14	0.12	0.12	0.10	0.12
MgO	5.90	5.5	5.9	5.6	6.8	5.8	4.5	6.2	6.0	12.0	12.4	5.1	5.2	7.1	7.2	8.0	6.4	6.3	6.3	5.6	6.0
CaO	9.7	9.6	10.0	9.9	9.4	9.3	9.3	10.8	11.2	10.0	8.6	6.8	7.6	9.2	9.3	8.7	5.8	6.8	7.3	7.0	6.8
Na_2O	2.85	2.83	2.78	2.84	2.64	3.24	3.10	3.00	2.65	2.30	2.00	2.81	2.74	2.44	2.44	2.80	2.83	2.90	3.00	4.00	3.20
K_2O	0.57	0.62	0.48	0.51	0.87	0.80	0.85	0.51	0.68	0.53	0.60	2.74	2.45	0.88	0.88	1.95	2.73	2.10	2.20	3.20	1.40
P_2O_5	0.14	0.12	0.11	0.12	0.11	0.11	0.20	0.11	0.11	0.10	0.11	0.48	0.47	0.16	0.16	0.48	0.46	0.45	0.50	0.46	0.46
H_2O	1.51	1.41	1.28	1.36	3.86	3.26	2.10	0.40	1.58	1.03	1.88	3.06	3.33	3.29	3.11	2.08	3.16	2.42	2.40	1.50	2.14
CO_2	0.58	0.46	0.40	0.41	1.03	0.32	0.43	0.56	0.30	0.71	0.36	0.38	1.01	0.67	0.70	1.26	0.14	0.22	0.51	0.14	0.40
Total	99.6	99.6	99.6	99.6	99.6	99.5	100.3	100.3	99.6	100.6	100.4	99.6	99.5	99.5	99.6	99.2	99.0	99.4	98.9	99.3	100.3
Ba	155	138	113	115	143	163	170	122	128	106	165	960	815	173	189	676	918	907	701	1662	500
Cr	134	98	155	121	149	167	40	132	140	1041	613	85	85	305	321	112	241	220	204	241	171
Ni	97	89	100	98	93	78	32	83	52	260	384	25	22	101	98	27	152	187	92	48	131
Rb	7	8	2	4	20	27	44	13	22	17	22	111	96	27	24	72	66	35	65	64	54
Sr	198	209	212	213	259	337	222	190	272	198	184	360	356	277	276	273	348	620	394	625	466
V	226	230	205	213	222	212	260	199	232	175	214.0	214	216	216	222	321	174	178	170	184	130
Zn	93	95	91	96	81	72	119	91	68	82.0	89.0	79	81	92	89	77	103	94	100	61	62
Zr	115	96	88	93	78	78	115	100	68.0	64.0	68.0	219	214	105	105	212	360	188	330	196	236
Y	22	19	19	20	14	14	25	18	14	14	16	31	29	17	18	56	35	24	28	29	26
Li	8	8	7	7	30	20	15	7	9	8	10	12	12.9	17	16	11.5	7.9	15.9	16.2	8.4	15.3
Nb	7.7	7	6.1	6.5	7.7	7.6	13	6.4	8.1	6.3	7.6	14	13	12	11	19	24	14.1	20.8	14	14.9
Mo	0.61	0.5	0.43	0.12	0.45	0.4	1.5	0.69	0.58	0.97	0.63	0.57	0.45	0.72	0.86	0.492	1.14	0.67	2.76	0.24	0.94
Cd	0.11	0.11	0.12	0.12	0.12	0.15	0.16	0.12	0.12	0.12	0.12	0.11	0.11	0.11	0.12	0.098	0.19	0.2	0.16	0.29	0.17
Cs	1.09	1.23	0.92	0.96	25	1.9	14	0.66	3.0	2.1	2.7	1.04	1.12	6.32	6.01	1.48	0.66	6.7	1.5	0.38	1.19

Pb	2.6	3.1	2.39	2.72	3.88	2.34	3.7	2.3	2.8	1.8	2.2	14.74	10.49	3.1	3.08	6.45	9.48	11.65	6.34	7.56	8.52
Th	2.04	1.84	1.57	1.59	1.19	1.17	2.9	1.8	1.9	1.7	1.9	11.11	10.46	2.03	2.17	9.15	10.16	11.95	8.41	15.15	7.04
U	0.47	0.48	0.38	0.39	0.32	0.31	0.69	0.40	0.51	0.34	0.43	1.35	1.34	0.53	0.54	1.77	1.77	1.9	1.9	2.21	1.09
Sc	23	23	23	23	25	24	22	23	24	24	24	30	29	26	25	89	27	22	23	24	20
Co	40	40	39	39	39	34	52	54	56	70	35	26	26	40	38	30	30	27	46	22	28
Cu	47	46	49	54	53	39	48	52	76	67	44	16	13	39	38	28	29	66	37	248	36
Ga	20	20	19	20	18	18	22	19	15	14	18	19	18	18	18	19	19	18	19	16	17
Sb	0.08	0.12	0.11	0.11	0.47	0.81	0.09	0.06	0.08	0.03	0.08	0.12	0.11	0.17	0.15	0.3	0.14	0.33	0.24	0.21	0.15
Sn	0.97	1.01	0.82	0.86	0.68	0.72	1.5	0.82	0.82	0.67	0.76	2.21	2.18	0.88	0.8	1.82	2.51	4.37	2.04	19.1	1.25
La	11	10	9	10	8	8	14	8.2	8.3	8	8.8	28	26	12	12	27	38	40	36	40	30
Ce	25	22	20	22	18	18	32	19	18	17	20	62	59	27	27	72	78	82	78	77	66
Pr	3	2.5	2.3	2.4	2.3	2.3	3.9	2.2	2.2	2.1	2.6	8.2	7.5	3.2	3.3	11	9.9	9.7	9.6	9.2	7.9
Nd	14	12	11	12	10	10	18	10	9.7	9.7	11	35	33	14	14	52	39	37	39	40	32
Sm	3.5	3.1	3	3.1	2.6	2.6	4.5	2.8	2.4	2.6	2.8	7.4	7.1	3.2	3.3	14	8	6.9	8.1	7.5	6.4
Eu	1.1	1.1	1.2	1.2	0.94	0.91	1.5	0.98	0.89	0.88	0.92	1.8	1.8	1	1.1	3.1	2	1.71	2.12	2.2	1.73
Gd	4.2	3.7	3.6	3.8	3	3	5.3	3.5	2.8	3.1	3.2	7	6.7	3.7	3.7	14	7.3	6.1	7.6	7	6.1
Tb	0.79	0.72	0.71	0.72	0.55	0.56	0.86	0.60	0.49	0.52	0.59	1.2	1.2	0.66	0.69	2.3	1.2	0.81	0.99	0.78	0.82
Dy	4.5	4	4	4.1	3	3	5.3	3.7	2.9	3.1	3.3	6.3	6	3.7	3.8	13	6.1	5.02	6.17	6	5.31
Ho	0.86	0.74	0.75	0.78	0.58	0.57	0.98	0.70	0.55	0.57	0.61	1.2	1.16	0.7	0.7	2.3	1.1	0.95	1.15	1.02	1
Er	2.6	2.3	2.3	2.3	1.7	1.7	2.9	2.1	1.6	1.7	1.8	3.6	3.4	2.1	2.1	6.6	3.2	2.67	3.14	3.02	2.86
Tm	0.37	0.32	0.32	0.33	0.24	0.25	0.38	0.31	0.24	0.23	0.24	0.49	0.49	0.29	0.31	0.91	0.43	0.36	0.44	0.41	0.4
Yb	2.3	2	2	2.1	1.5	1.6	2.5	1.9	1.5	1.4	1.6	3.4	3.2	1.9	1.9	5.5	2.9	2.45	2.81	2.4	2.69
Lu	0.32	0.28	0.28	0.29	0.21	0.21	0.35	0.27	0.21	0.20	0.23	0.47	0.46	0.25	0.26	0.79	0.42	0.35	0.4	0.43	0.39
Mg#	49.9	47.6	49.8	48.18	56.97	53.83	38.25	51.2	54.3	66.85	65.94	52.4	52.8	55.6	55.9	60.5	55.7	59.2	56.7	60.5	56.68

Samples of 7 to 10 major elements after Kramer (1988). gb: gabbros; peg-gb: pegmatitic gabbro; ol-gb: olivine gabbros; dt: diorite; sp.: spessartites. Locations: samples VG1, VG2, VG3, VG4 and VG8 from Valtengrund; KE5 and KE6 from Klunst Ebersbach; BS7 from Bautzen-Stiebitz; SH9 and SH11 from Soraer Höhe; FB10 from Fichtenberg; DG12, DG13 and DG17 from Das Gericht; JS14, JS15, JS16 and JS18 from Julienstein; SW19 from Strahwalde; HB20 from Hutzelberg; IS21 from Israel.

(Fig. 5), they straddle the boundary between the alkaline and the sub-alkaline series similar to the lamprophyres from the adjacent areas and plot in the fields of trachybasalts, basaltic andesites, basaltic trachyandesites, and basalts. The Lusatian lamprophyres show lower alkali and silica contents relative to the lamprophyres from the adjacent areas (Fig. 5).

The gabbros generally have lower Mg# (38–57), MgO (4.4–6.2 wt.%), Cr (40–167 ppm), and Ni (52–100 ppm) than the calc-alkaline lamprophyres (Mg# 52–61, MgO 5.1–8 wt.%, Cr 85–321 ppm, Ni 22–187 ppm), except for two gabbroic samples that have high Mg# and high MgO, FeO, Cr, and Ni contents as the result of olivine accumulation. The gabbros have high contents of CaO (9.3–11.2 wt.%). The calk-alkaline lamprophyres are characterized by moderate contents of Al_2O_3 (14.3–16.9 wt.%), TiO_2 (1–2.46 wt.%), and CaO (5.7–9.1) and high contents of K_2O (0.88–3.20 wt.%). Furthermore, the calc-alkaline lamprophyres have greater abundances of Rb (24–111 ppm), Zr (105–360 ppm), Nb (11–20.8 ppm), Ba (173–1662 ppm), Pb (3.1–14.7 ppm), Th (2–15.2 ppm), and Sr (273–625 ppm) than the gabbros (Rb 2–44 ppm, Zr 64–115 ppm, Nb 6.1–8.1 ppm, Ba 106–170 ppm, Pb 1.8–3.9 ppm, Th 1.2–2.9 ppm, and Sr 198–337 ppm).

Trace element variation diagrams show no systematic variations of Zr, Rb, Sr, and Nb with SiO_2 for gabbros and calc-alkaline lamprophyres (Fig. 4). The gabbros cluster in a relatively narrow field, whereas the calc-alkaline lamprophyres typically have higher trace element and SiO_2 contents (Fig. 4). Only two spessartite samples overlap with the gabbro composition.

In multi-element variation diagrams, gabbros and calc-alkaline lamprophyres from Lusatia show a strong enrichment relative to primitive mantle (Fig. 6a). Both groups show a similar pattern with a significant Nb trough, although the calc-alkaline lamprophyres have distinctly higher trace element contents (i.e., U, Pb, Th, Ti, Ba, Rb, Cs, Zr, and Nb). The rare earth element pattern of the gabbros is steeper compared to the average N-MORB, showing slightly relative light rare earth element (LREE) enrichment and heavy rare earth element (HREE) depletion (Fig. 6b). The gabbros are strongly enriched in large-ion lithophile elements (i.e., the LILE—Cs, Pb, Rb, Ba, Sr) relative to N-MORB (Fig. 6a). The gabbros show slightly less enriched Nb contents than those of U and La (Fig. 6a). The calc-alkaline lamprophyres show a stronger enrichment in Rb/Nb and Ba/Nb than the gabbros. Furthermore, the calc-alkaline lamprophyres exhibit a strong Pb peak, and a slight trough in Sr relative to Pb and Nd concentrations. A similar geochemical fingerprint has been documented for late-Variscan lamprophyres of the Black Forest (Hegner et al., 1998; Fig. 6a), the Sudetes (Awdankiewicz, 2007), and the Erzgebirge (Seifert, 2008) and alkaline basalts and Cretaceous ultramafic lamprophyres of Lusatia (Renno et al., 2003a,b; Abdelfadil et al., 2010) and Saxo-Thuringian upper crust (Romer and Hahne, 2010).

Chondrite normalized REE pattern for gabbros and calc-alkaline lamprophyres (Fig. 6b) exhibit strong enrichment in LREE with La abundances up to 200 times chondritic values (Sun and McDonough, 1989). REE pattern for the gabbros are moderately fractionated with $(La/Yb)_N = 3–3.8$, whereas those for the calc-alkaline lamprophyres are strongly fractionated with $(La/Yb)_N = 3.3–11$. The HREE in the gabbro samples are less enriched than those in the calc-alkaline lamprophyres. There is no Eu anomaly in gabbro and calc-alkaline lamprophyre samples, except for one lamprophyre sample that has a slightly negative Eu anomaly. The calc-alkaline lamprophyres of Lusatia have a similar REE pattern as lamprophyres from the Black Forest (Hegner et al., 1998), but a flatter REE pattern (i.e., lower LREE) than lamprophyres from the Erzgebirge (Seifert, 2008) and the Sudetes (Awdankiewicz, 2007; Fig. 6b).

The Nd, Sr, and Pb isotopic compositions of gabbros and calc-alkaline lamprophyres are presented in Table 4. Gabbros and calc-alkaline lamprophyres encompass a relatively wide range of measured Sr isotopic compositions from 0.7048 to 0.7074 and 0.7061 to 0.7119, respectively. The gabbros show a narrow range of measured Nd isotope compositions from 0.51256 to 0.51268, whereas the calc-alkaline lamprophyres show a broader variation from 0.51225 to 0.51265. The Nd isotopic composition of the gabbros falls in the compositional range of the depleted mantle, although the trace-element signatures and to a lesser extent from the Sr isotopic compositions indicate that this mantle had been affected by metasomatic additions of evolved material. The calc-alkaline lamprophyres fall between the compositions of depleted mantle and the Saxo-Thuringian upper crust (Linnemann and Romer, 2002; Romer and Hahne, 2010) in the εNd_{init} vs. $^{87}Sr/^{86}Sr_{init}$ diagram (Fig. 7a). The measured Pb isotope composition of the gabbros and calc-alkaline lamprophyres exhibit relatively wide compositional variations with $^{206}Pb/^{204}Pb = 18.16–18.97$, $^{207}Pb/^{204}Pb = 15.55–15.64$, and $^{208}Pb/^{204}Pb = 38.35–39.93$ (Table 4). The Pb from both gabbros and lamprophyres have at a given $^{206}Pb/^{204}Pb_{init}$ far higher $^{207}Pb/^{204}Pb_{init}$ than the mantle, i.e., their Pb is dominated by crustal Pb (Fig. 7b). The calc-alkaline lamprophyres, however, have higher $^{207}Pb/^{204}Pb_{init}$ ratios than the gabbros for corresponding $^{206}Pb/^{204}Pb_{init}$, indicating that crustal contributions to the lamprophyres (and their source) are much more prominent than to the gabbros.

5. Discussion

5.1. Alteration and assimilation processes

Alteration of minerals is typical in lamprophyres and could affect also the element and isotope geochemistry of the whole-rock samples (Rock, 1977; Turpin et al., 1988). The samples used for geochemical analysis are fresh and show no systematic correlation between LOI and Sr isotopic composition (not shown), except for sample DG12, which has the highest $^{87}Sr/^{86}Sr$ value (0.71194), a high LOI of 3.44 wt.%, and Rb contents of 111 ppm. These features may be ascribed to alteration. Similarly, the two olivine gabbro samples (KE5, KE6) with the highest LOI (3.58 wt.% and 4.89 wt.%, respectively) show the most radiogenic Sr isotopic compositions for gabbro (0.70601 and 0.70635, respectively). The association of high volatile content and radiogenic Sr isotopic composition indicates that fluids released from the wall-rocks during emplacement of the gabbros and the lamprophyres have transported radiogenic Sr – also derived from the wall-rocks – into the magmatic rocks. In addition, the highest LOI, Sr, and Rb samples show a similar range of Nd isotopic ratios as samples with lower contents of LOI. To avoid effects of fluid–rock interaction during emplacement, only immobile elements were used for petrogenetic interpretations.

The crustal geochemical fingerprints in the gabbros and the calc-alkaline lamprophyres may be the result of two types of processes (and their combination). The first type of process is related to the ascent and emplacement of the magma, i.e., differentiation of basic magma by fractional crystallization (FC; e.g., Kramer, 1976; Currie and Williams, 1993) and assimilation of country rocks with fractional crystallization (AFC; e.g., DePaolo, 1981). The second type of processes involves the modification of the mantle source by subduction-related fluids/melt (Condie, 1990; Feng et al., 2004; Prelević et al., 2005; Awdankiewicz, 2007; Nédli and Tóth, 2007).

Using incompatible trace elements to distinguish between fractional crystallization, assimilation with fractional crystallization, and mixing processes (e.g., DePaolo, 1981; Cribb and Barton, 1996), we modeled FC and AFC processes (Fig. 8). This modeling demonstrates that fractional crystallization and assimilation with fractional crystallization cannot account for the observed variation within the data and indicates that two source components are better suited to explain the geochemical and isotopic variability among the samples. The key results of the modeling are:

(i) The scattered variation of initial $^{87}Sr/^{86}Sr$ with MgO concentration (Fig. 9a) cannot be obtained by AFC. Assimilation of crustal rocks will decrease MgO and increase $^{87}Sr/^{86}Sr$. Similarly, FC would result in lower MgO at constant Sr isotopic composition.

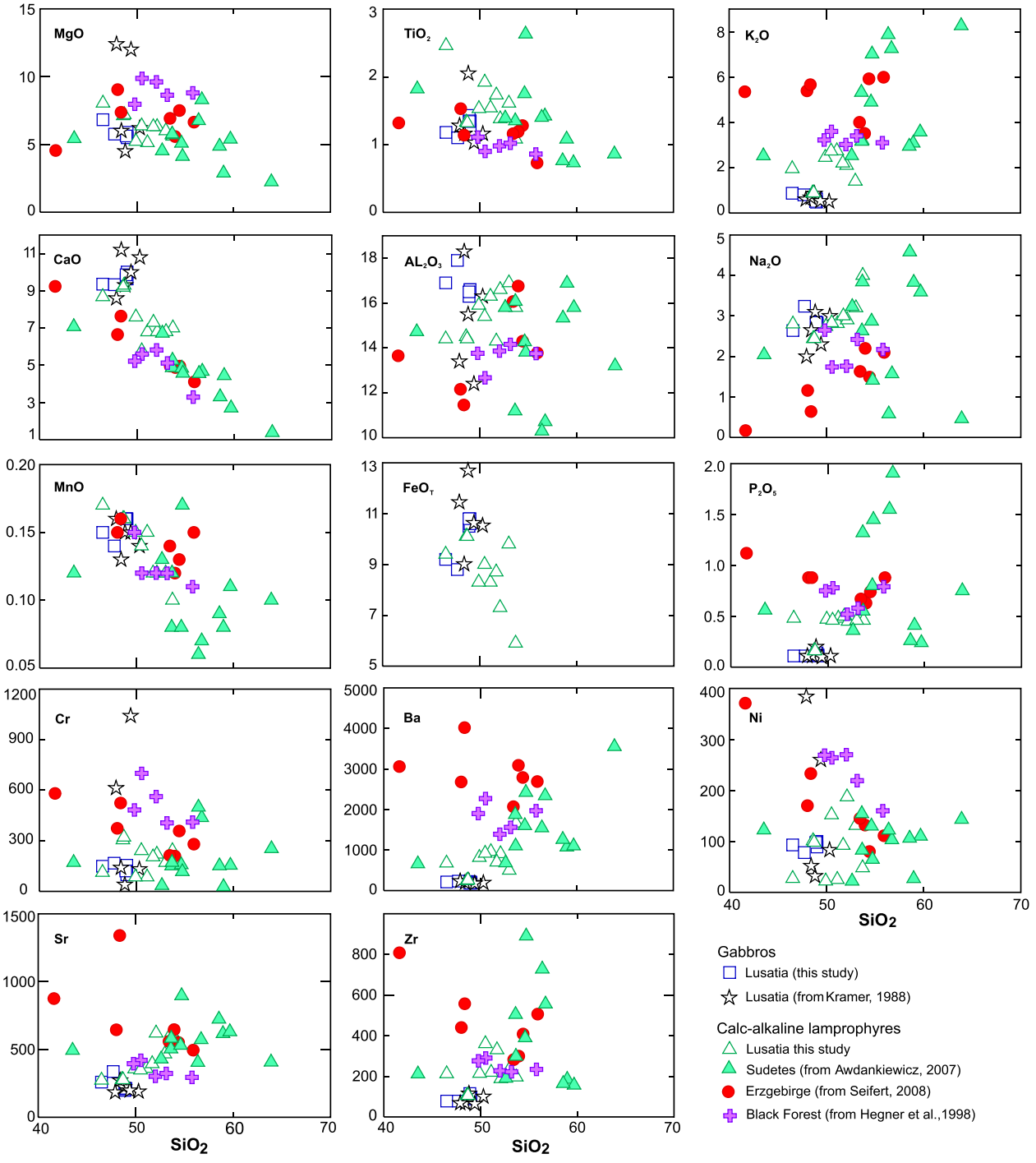

Fig. 4. Major (wt.%) and trace element (ppm) composition of Lusatian gabbros and lamprophyres compared with those from other regions. Data sources: gabbros—Kramer (1988); lamprophyres from the Sudetes—Awdankiewicz (2007); lamprophyres from the Erzgebirge—Seifert (2008) and lamprophyres from the Black Forest—Hegner et al. (1998).

(ii) The strong enrichment in LREE and LILE (Fig. 6a, b) in combination with low Ce/Pb and high Mg# and compatible element (e.g., Cr, Ni, MgO; Fig. 4) contents cannot be obtained by AFC processes.

(iii) The absence of regular trends in binary diagrams of gabbros and spessartites (Fig. 4) and the more radiogenic Sr and Pb isotopic composition and the lower $^{143}Nd/^{144}Nd$ ratios (Fig. 7) of the lamprophyres in comparison to the gabbros do not support a derivation of spessartite by fractionation from the gabbro source as suggested by Kramer (1976) and Currie and Williams (1993). In particular, continued development of the Sr, Nd, and Pb isotopic composition in the gabbro source from the time of gabbro extraction to the time of lamprophyre emplacement cannot account for the contrasting isotopic compositions of gabbros and lamprophyres.

5.2. Pre/late Variscan geochemical fingerprints of the mantle beneath Lusatia

The pre-Variscan gabbros have Nb/U, Ce/Pb, Th/La, Sm/La and Ba/Nb ratios that resemble crust rather than mantle and that demonstrate the involvement of crustal material in the mantle source of the gabbros

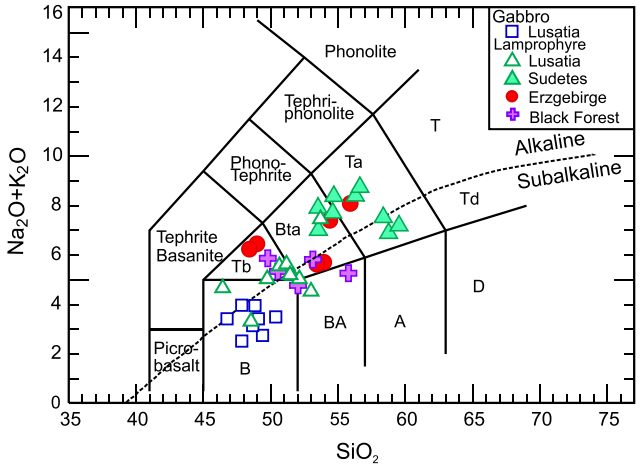

Fig. 5. The total alkali versus silica (TAS) diagram (Le Maitre et al., 2002), with selected fields annotated: A (andesites), B (basalts), BA (basaltic andesites), BTa (basaltic trachyandesites), D (dacites), R (rhyolites), T (trachytes), Ta (trachyandesites), Tb (trachybasalts).
The boundary between the alkaline and subalkaline series is after Irvine and Baragar (1971). Data sources of the lamprophyres from the adjacent areas are as in Fig. 4.

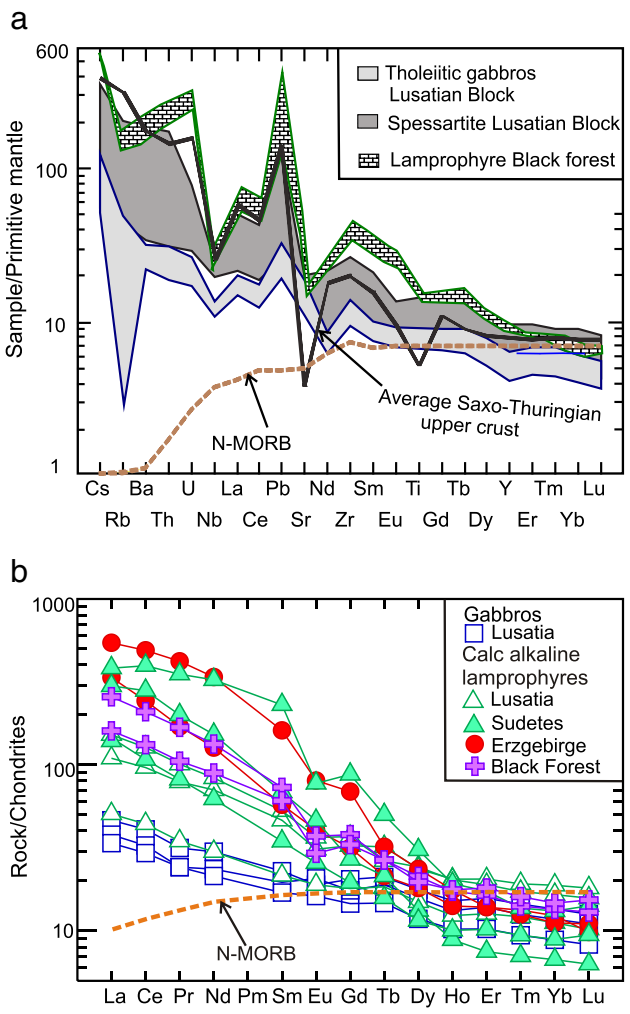

Fig. 6. a) Primitive-mantle-normalized pattern (Sun and McDonough, 1989); and b) chondrite-normalized patterns (Sun and McDonough, 1989) of Lusatian gabbros and calc-alkaline lamprophyres from Variscan Massifs.
Data sources: N-MORB—Sun and McDonough (1989); lamprophyres from the Sudetes—Awdankiewicz (2007); lamprophyres from the Erzgebirge—Seifert (2008); lamprophyres from the Black Forest—Hegner et al. (1998). Saxo-Thuringian upper crust from Romer and Hahne (2010) is shown for reference. Some calc-alkaline lamprophyres from Sudetes with the most extreme pattern are described as lamproites (Krmíček, 2010).

(Fig. 9). The transfer of crustal signatures from subducted rocks to the mantle is a selective process that depends on the devolatization and melting history of the subducted material. Thus it does not impose crustal trace-element signatures completely unchanged to the metasomatized mantle. The striking similarity of the trace element patterns of Saxo-Thuringian upper crust and lamprophyres with Nb, Sr, Pb, and Zr anomalies (Fig. 6a) reflects that rocks with this regionally occurring geochemical signature have modified the lamprophyre source. The contrasting enrichment or depletion of trace element abundance in the mantle normalized pattern in Variscan lamprophyres from Lusatia and from other areas (e.g., Sudetes, Black Forest, French Massif Central) indicates both the heterogeneity of the mantle source and regionally variable contribution of the subducted crustal material. Crustal contributions to the gabbro source are also evident in a trace element pattern normalized to continental crust (Fig. 10a), as the gabbros have a flat pattern with marked depletions in Pb and Rb and slight enrichments in Cs, and Sr. The crustal Pb isotopic compositions and the high initial $^{87}Sr/^{86}Sr$ values of the gabbros at essentially constant initial $^{143}Nd/^{144}Nd$ values indicate fluid-mediated uncoupling of Pb and Sr from Nd (Fig. 7a, b). The tholeiitic gabbros in the Lusatian Block show a marked geochemical contrast to the c. 400 Ma old gabbros of the adjacent Sudetes that show N-MORB affinity, εNd_{400} (8.1 to 8.5) and Sr isotopes (0.7021 to 0.7028; Fig. 7a) and are considered to be a part of an ophiolite complex (Kryza and Pin, 2010). Thus, the geochemical signature of the Lusatian gabbros reflects a mantle source that has been metasomatized during subduction related to the Cadomian orogeny.

The late-Variscan calc-alkaline lamprophyres show a trace element pattern characteristic for the involvement of crustal material in their source, with their high Rb, Ba, Pb, Sr, U, Th, and Cs contents, high Th/La, and low Sm/La (Fig. 9d). Furthermore, their Ba/Nb (14.4–118), Nb/U (6.35–22.6), Th/U (3.8–8.2), Th/Nb (0.17–1.08), and Ce/Pb (4–12) ratios are typical for continental crust (e.g., Taylor and McLennan, 1995) and their trace element pattern resembles Saxo-Thuringian upper crust (Fig. 6a), i.e., the rocks that are supposed to have been subducted during the Variscan orogeny (e.g., Mingram, 1998; Kroner and Romer, 2010; Rötzler and Plessen, 2010).

5.3. Repeated mantle-metasomatism beneath Lusatia

Even, the crustal signature of late-Variscan calc-alkaline lamprophyres of Lusatia is distinct from the pre-Variscan gabbros by high initial $^{87}Sr/^{86}Sr$, $^{207}Pb/^{204}Pb$, and $^{206}Pb/^{204}Pb$ ratios and low $^{143}Nd/^{144}Nd$ ratios (εNd_{330} range from +2.5 to −4.9) (Fig. 7a), they both have crustally influenced Pb (Fig. 7b). The higher $^{207}Pb/^{204}Pb$ values at similar $^{206}Pb/^{204}Pb$ values in most spessartite samples than for the majority of the gabbro samples indicates that the spessartites generally have higher input of crustal Pb. The shift of the initial Pb of the spessartites of Lusatia to higher $^{206}Pb/^{204}Pb$ values is due to the younger age of the spessartites and reflects Pb growth in the spessartite source from the time of gabbro formation to the time of spessartite formation. The higher $^{207}Pb/^{204}Pb$ values in lamprophyres from the Erzgebirge, the Black Forest, and the French Massif Central reflects the larger contribution of crustal Pb in the source of these rocks than in the source of the Lusatian spessartites.

The $^{143}Nd/^{144}Nd$ and $^{87}Sr/^{86}Sr$ ratios of the gabbros (and more importantly their source) range at 330 Ma from 0.51222 to 0.51234 and from 0.7036 to 0.7064, respectively, which is generally lower from the one of the lamprophyres at 330 Ma (0.51198–0.51234 and 0.7046–0.7080, respectively). The lamprophyres cannot be extracted from the same source as the gabbros, as the 330 Ma old spessartites with the least radiogenic initial Nd have lower $^{143}Nd/^{144}Nd$ values

Table 4
Whole-rock Sr, Nd, and Pb isotope data of gabbros and calc-alkaline lamprophyres from Lusatia, Germany.

	Sample[a]	Age (Ma)	^{87}Sr [b] / ^{86}Sr	$^{87}Sr_{(T)}$ [c] / ^{86}Sr	^{143}Nd [b] / ^{144}Nd	$\varepsilon Nd_{(T)}$ [c]	^{206}Pb [d] / ^{204}Pb	^{207}Pb [d] / ^{204}Pb	^{208}Pb [d] / ^{204}Pb	^{206}Pb [e] / ^{204}Pb	^{207}Pb [e] / ^{204}Pb	^{208}Pb [e] / ^{204}Pb
1	VG1	330	0.705136 ± 5	0.70466	0.512593 ± 7	1.0	18.475	15.611	39.221	17.86	15.58	38.36
		400		0.70455		1.4				17.73	15.57	38.18
2	VG2	330	0.705217 ± 4	0.70470	0.512568 ± 4	0.3	18.272	15.566	38.455	17.76	15.54	37.82
		400		0.70459		0.7				17.65	15.53	37.68
3	VG3	330	0.704793 ± 4	0.70466	0.512573 ± 3	0.1	18.411	15.576	38.695	17.87	15.55	37.98
		400		0.70464		0.4				17.76	15.54	37.83
4	VG4	330	0.704955 ± 3	0.70470	0.512670 ± 4	2.3	18.241	15.553	38.427	17.77	15.53	37.80
		400		0.70465		2.7				17.66	15.52	37.66
5	KE5	330	0.707064 ± 6	0.70601	0.512680 ± 4	2.5	18.157	15.588	38.348	17.88	15.57	38.02
		400		0.70579		2.8				17.82	15.57	37.95
6	KE6	330	0.707441 ± 4	0.70635	0.512642 ± 4	1.7	18.250	15.566	38.353	17.82	15.54	37.82
		400		0.70612		2.1				17.72	15.54	37.70
7	SH9	330	0.704856 ± 4	0.70448	0.512658 ± 6	2.4	18.331	15.559	38.517	17.72	15.53	37.79
		400		0.70438		2.8				17.59	15.52	37.63
8	BS7	330	0.706281 ± 5	0.70359	0.512646 ± 5	2.1	18.395	15.558	38.570	17.77	15.53	37.72
		400		0.70301		2.5				17.64	15.52	37.54
9	VG8	330	0.704869 ± 4	0.70394	0.512613 ± 5	0.7	18.338	15.553	38.529	17.76	15.52	37.68
		400		0.70374		0.9				17.63	15.51	37.50
10	DG12	330	0.711938 ± 2	0.70775	0.512256 ± 5	−4.6	18.334	15.591	38.991	18.03	15.58	38.17
11	DG13	330	0.711637 ± 4	0.70797	0.512259 ± 5	−4.6	18.470	15.602	39.218	18.04	15.58	38.13
12	JS14	330	0.706119 ± 5	0.70479	0.512608 ± 4	1.9	18.368	15.568	38.541	17.80	15.54	37.83
13	JS15	330	0.706116 ± 6	0.70493	0.512651 ± 3	2.5	18.379	15.566	38.548	17.80	15.54	37.79
14	JS18	330	0.708408 ± 5	0.70764	0.512356 ± 6	−2.0	18.635	15.603	39.008	18.09	15.57	37.89
15	SW19	330	0.707204 ± 4	0.70496	0.512476 ± 7	−0.1	18.860	15.594	39.160	17.85	15.54	37.71
16	DG17	330	0.707592 ± 5	0.70501	0.512472 ± 4	−0.2	18.888	15.620	39.236	18.25	15.59	38.06
17	HB20	330	0.708766 ± 4	0.70737	0.512299 ± 6	−3.1	18.970	15.640	39.928	17.97	15.59	37.70
18	IS21	330	0.706213 ± 5	0.70463	0.512514 ± 5	0.7	18.534	15.606	38.904	18.10	15.58	38.01

[a] Sr, Nd and Pb isotopic compositions were analyzed at Deutsches GeoForschungsZentrum GFZ (Potsdam). The samples were dissolved with concentrated HF for four days at 160 °C on the hot plate. The digested samples were dried, taken up in 2 N HNO_3 and slowly dried then the samples were taken up in 6 N HCl.

[b] $^{87}Sr/^{86}Sr$ and $^{143}Nd/^{144}Nd$, normalized to $^{86}Sr/^{88}Sr = 0.1194$ and $^{146}Nd/^{144}Nd = 0.7219$, respectively, were obtained on a Thermo Triton and a Finnigan MAT262 multi-collector mass-spectrometer, respectively, using dynamic multicollection. Analytical uncertainties are given at $2\sigma_m$ level.

[c] $^{87}Sr/^{86}Sr_{(T)}$ and $\varepsilon Nd_{(T)}$ were calculated for the emplacement age using $\lambda^{87}Rb = 1.42E\text{-}11\ y^{-1}$ and $\lambda^{147}Sm = 6.54E\text{-}12\ y^{-1}$, $(^{147}Sm/^{144}Nd)^0_{CHUR} = 0.1967$, and $(^{143}Nd/^{144}Nd)^0_{CHUR} = 0.512638$, respectively, and the concentration data given in Table 3.

[d] Pb was separated and purified using ion-exchange chromatography as described in Romer et al. (2005). The Pb isotopic composition was determined on a Finnigan MAT262 multi-collector mass-spectrometer using static multicollection. Lead isotope data corrected for mass discrimination with 0.1%/A.M.U. as estimated from the repeated measurement of lead reference material NBS 981. Reproducibility at 2σ level is better than 0.1%.

[e] Lead isotope data recalculated to the emplacement age using the contents of Pb, Th, and U (Table 3) and the constants recommended by IUGS ($\lambda^{232}Th = 4.9475E\text{-}11\ y^{-1}$, $\lambda^{235}U = 9.8485E\text{-}10\ y^{-1}$, and $\lambda^{238}U = 1.55125E\text{-}10\ y^{-1}$).

than the 400 Ma old gabbros at the time of their extraction from the mantle. Thus to serve also as source for the spessartites, the gabbro source had to experience Variscan metasomatism accounting for the less radiogenic Nd isotopic compositions.

The similarity of high Cr, MgO, Mg#, the trace-element pattern (Fig. 4, 6a) and Th/La, Sm/La, and Ce/Pb ratios (Fig. 9) indicates that gabbros and calc-alkaline lamprophyres have been extracted from a similar mantle source, whereas the contrasting isotopic compositions of Sr and Nd indicates that this source either was heterogeneous or that there was a second, i.e., Variscan, event of mantle enrichment.

Melting of heterogeneous (veined) mantle with depleted and metasomatically enriched domains will result in the preferential melting of the metasomatized domains. These melts will react with the depleted mantle and induce melting of the depleted mantle and lead to rocks with a depleted geochemical signature for the compatible elements (high Cr, Ni, Mg, Mg#) and enriched trace element signatures for incompatible elements (e.g., Foley, 1992; Tappe et al., 2008). For a small degree of melting, the metasomatic component will be more prominent than for a large degree of melting. Thus, the isotopic and geochemical fingerprints of incompatible elements are less prominent in melts reflecting a high degree of melting. Thus, the contrasting degree of melting could account for some differences between the isotopic composition and geochemical signatures of gabbros and calc-alkaline lamprophyres.

Melting of the mantle to produce the gabbros, however, would result in the preferential melting of the metasomatized domains and leaving behind a mantle that is depleted in incompatible elements. Renewed small-scale melting of this mantle would not produce a melt that is highly enriched in incompatible elements, as the metasomatized parts of the mantle that could provide these elements have been consumed during the melting of the gabbro source. Thus, the late-Variscan lamprophyres require a refertilization of the mantle after the extraction of gabbro melts. The two events possibly account for the contrasting positions occupied by the gabbros and the calc-alkaline lamprophyres in the Th–Zr–Nb discrimination diagram (Fig. 10b) with the systematically stronger Th enrichment and Nb depletion in the calc-alkaline lamprophyre than in the gabbros.

Variscan mantle enrichment has also been inferred for the source of other lamprophyre occurrences throughout the Variscan orogen, typically stressing the predominance of geochemical fingerprints inherited from melted sedimentary rocks (Turpin et al., 1988; Awdankiewicz, 2007). In addition, the lamprophyres of Lusatia show similar $^{87}Sr/^{86}Sr$ and εNd_{330} values as the calc-alkaline lamprophyres from the Sudetes (Awdankiewicz, 2007) and the French Massif Central (Turpin et al., 1988), but have lower $^{87}Sr/^{86}Sr$, $^{207}Pb/^{204}Pb$, and $^{206}Pb/^{204}Pb$ and higher εNd_{330} values than calc-alkaline lamprophyres from the Black Forest (Hegner et al., 1998) and adjacent Erzgebirge (Fig. 7a, b), which may reflect more extensive metasomatism in the lamprophyre source of the Erzgebirge. Minettes are also derived from a Variscan metasomatized mantle source, although the metasomatic fluids have been interpreted to be derived from recycled continental crust (Hoch

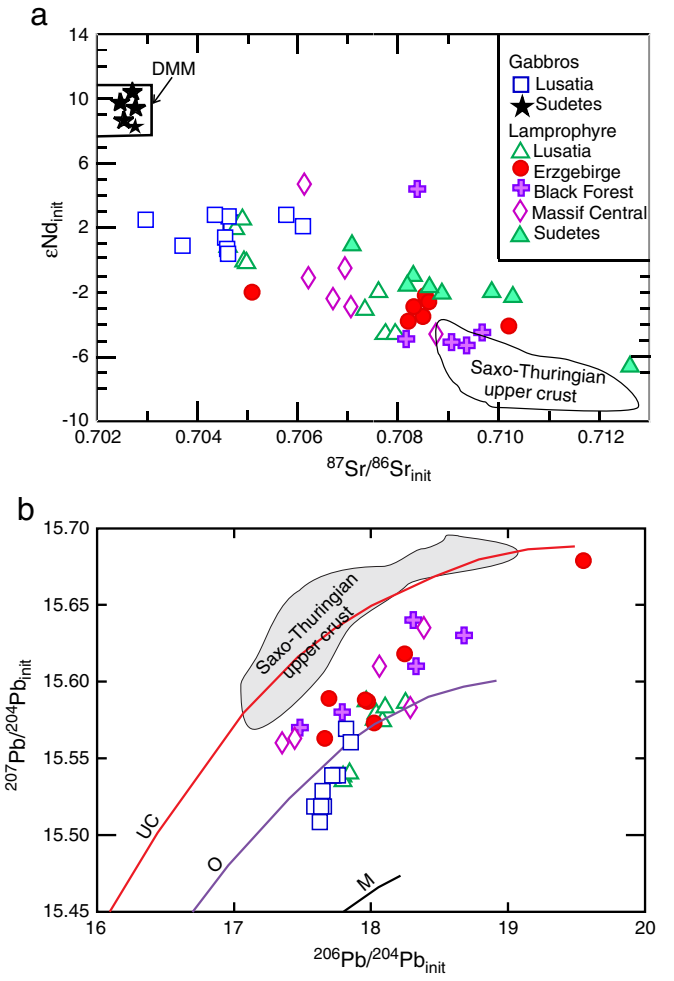

Fig. 7. a) The εNd_{init} versus $^{87}Sr/^{86}Sr_{init}$ and b) initial Pb isotopic composition of Lusatian lamprophyres and gabbros compared with late and post-Variscan lamprophyres from the Sudetes (Awdankiewicz, 2007), the Erzgebirge (Seifert, 2008), the Black Forest (Hegner et al., 1998), the French Massif Central (Turpin et al., 1988), gabbros from the Sudetes (Pin et al., 1988), and Saxo-Thuringian upper crust (Romer and Hahne, 2010). Note the gabbros are recalculated to 400 Ma, whereas the lamprophyres are calculated to 330 Ma. Depleted MORB mantle (DMM) are from Zindler and Hart (1986). Mantle (M), orogene (O) and upper crust (UC) Pb evolution curves are after Zartman and Doe (1981).

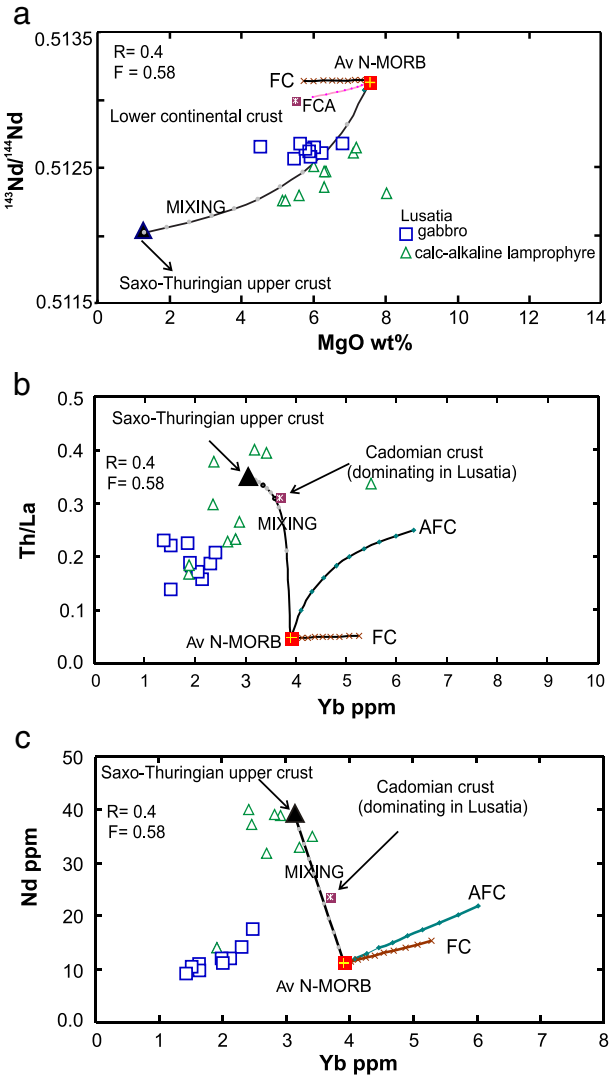

Fig. 8. (a) $^{143}Nd/^{144}Nd$ versus MgO (b) plots showing the results of FC, AFC, FCA, and mixing modeling results. C_0 = N-MORB average is from Hofmann (1988), Ito et al. (1987), and Hauri and Hart (1997); MgO = 7.57, Th = 0.187, La = 3.89, Nd = 11.18, Yb = 3.9 and $^{143}Nd/^{144}Nd$ = 0.5131. Saxo-Thuringian upper crust is from Romer and Hahne (2010). Two assimilants have been used; average lower continental crust is from Taylor and McLennan (1995) and Cadomian crust is from Linnemann and Romer (2002). Bulk partition coefficient; Kd_{La} = 0.182, Kd_{Th} = 0.028, Kd_{Nd} = 0.300, Kd_{Yb} = 0.323 and Kd_{MgO} = 0.249, which are calculated for the fractionating mineral assemblage of $plagioclase_{(0.6)}$, $clinopyroxene_{(0.2)}$, and $olivine_{(0.2)}$ in a basic magma. Fractional crystallization assimilation (FCA).

et al., 2001). Thus, the key message is not that there is a Variscan metasomatism of the mantle, but that there was already an earlier metasomatic event and that mantle can be repeatedly refertilized: in the special case of Lusatia, by a Cadomian metasomatism recorded by the post-Cadomian/pre-Variscan tholeiitic gabbros and by Variscan metasomatism recorded by the late-Variscan lamprophyres.

6. Conclusions

The mantle beneath Lusatia was modified by Cadomian (c. 600–570 Ma) and Variscan (c. 380–340 Ma) subduction. The metasomatic signature of this mantle was inherited by intra-plate magmatism at c. 400 Ma (gabbros) and c. 330 Ma (calc-alkaline lamprophyres). The effect of assimilation, alteration, and fractional crystallization as a source for the enrichment may be limited and the geochemical and isotopic signatures of these rocks were mainly inherited from an earlier subduction event by transferring the subducted materials as partial melts, which will not have the same compositions as the bulk subducted materials, but it will metasomatize the mantle. The pre-Variscan gabbros and the late-Variscan calc-alkaline lamprophyres in Lusatia were derived from the same mantle source. The calc-alkaline lamprophyres of Lusatia show the mantle enrichment much more distinctly than the gabbro, which indicates an enrichment of the mantle source after gabbro extraction during the Variscan orogeny and implies a repeatedly enriched mantle source. This is also supported by the similar age of the Lusatian calc-alkaline lamprophyres with the lamprophyres from the Central Europe (300–330 Ma) (e.g., Erzgebirge, Sudetes, and Black Forest). The lamprophyres have high large ion lithophile element contents (up to 350 times primitive mantle), high LREE/HREE, and elevated high-field-strength element contents, and crust-like Nd and Sr isotopic signatures. Their trace element pattern is similar to Saxo-Thuringian upper crust. A similar pattern also is observed for lamprophyres from the adjacent Sudetes, Black Forest,

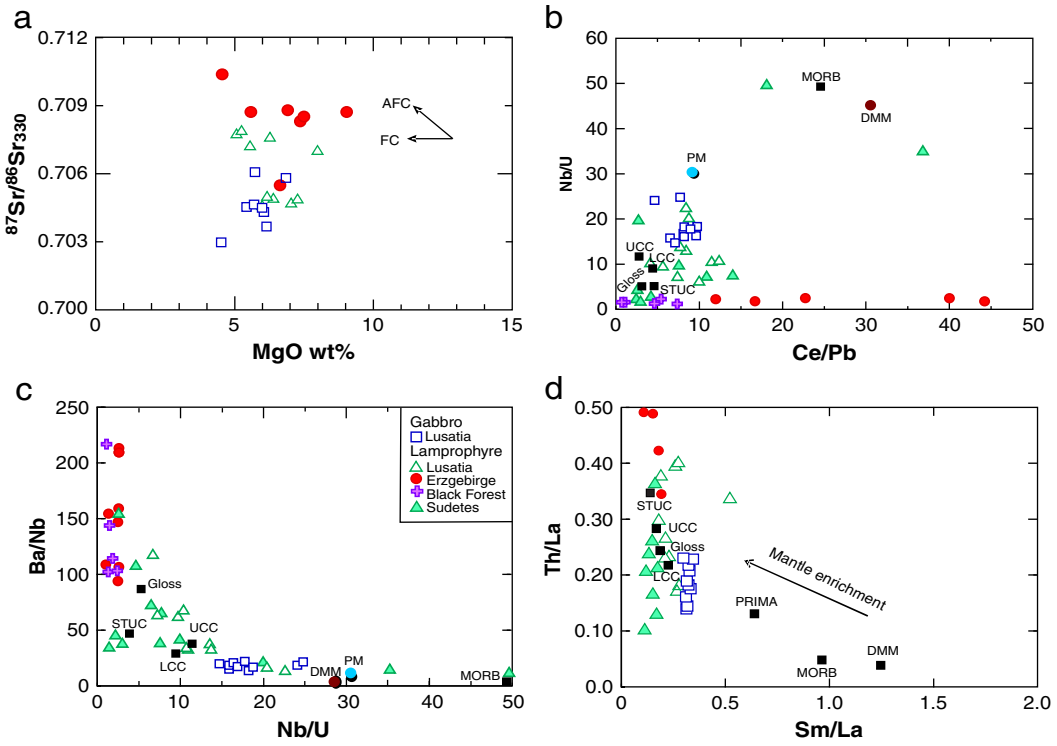

Fig. 9. (a) $^{87}Sr/^{86}Sr_{330}$ vs. MgO showing the effect of the FC and AFC; (b) Nb/U vs. Ce/Pb, (c) Ba/Nb vs. Nb/U, and (d) Th/La vs. Sm/La of the gabbros and the calc-alkaline lamprophyres. Average continental crustal compositions of lower (LCC) and upper crusts (UCC) are from Rudnick and Fountain (1995); primitive mantle (PM) from Hofmann (1988); global subducting sediment (GLOSS) from Plank and Langmuir (1998); Saxo-Thuringian upper crust (STUC) from Romer and Hahne (2010); mid-ocean ridge basalts (MORB) and primitive mantle from Hofmann (1988) and average depleted MORB mantle (DMM) from Workman and Hart (2005). Data sources are as in Fig. 6.

French Massif Central, and Erzgebirge regions. The different enrichment extent between late-Variscan lamprophyres in different domains in Central Europe reflects the regional heterogeneous effect of the Variscan orogeny.

Acknowledgments

We thank the academic and technical staff at Deutsches GeoForschungsZentrum for help with the analytical work, especially, R. Naumann for the XRF analysis, K. Hahne for trace element analysis, S. Tonn for REE data, and O. Appelt for support with the microprobe work. We thank M. Sudo for help with the Ar-dating of the two amphibole samples. K.M.A. gratefully thanks W. Kramer for guidance in the field. We gratefully acknowledge detailed and constructive reviews by L. Krmíček and two anonymous reviewers and thoughtful editorial comments by D. Prelević.

References

Abdelfadil, Kh., Romer, R.L., Seifert, Th., Lobst, R., 2010. Geochemistry and petrology of alkaline basalt and ultramafic lamprophyre dikes from Lusatia (Lausitz), Germany. Mineralogia Special Paper 37, 17–18.

Awdankiewicz, M., 2007. Late Palaeozoic lamprophyres and associated mafic subvolcanic rocks of the Sudetes (SW Poland): petrology, geochemistry and petrogenesis. Geol. Sudetica 39, 11–97.

Bédard, J.H., 1994. Mesozoic east North American alkaline magmatism: Part 1. Evolution of Monteregian lamprophyres, Québec, Canada. Geochimica et Cosmochimica Acta 58, 95–112.

Buzzi, L., Gaggero, L., Grozdanov, L., Yanev, S., Slejo, F., 2010. High-Mf potassic rocks in the Balkan segment of the Variscan Belt (Bulgaria); implications for the genesis of orogenic lamproite magmas. Geological Magazine 147, 434–450.

Condie, K.C., 1990. Growth and accretion of continental crust: inferences based on Laurentia. Chemical Geology 93, 183–194.

Cribb, J.W., Barton, M., 1996. Geochemical effects of decoupled fractional crystallization and crustal assimilation. Lithos 37, 293–307.

Currie, K.L., Williams, P.R., 1993. An Archean calc-alkaline lamprophyre suite, northeastern Yilgarn block, Western Australia. Lithos 31, 33–50.

DePaolo, D.J., 1981. Trace element and isotopic effects of combined wallrock assimilation and fractional crystallization. Earth and Planetary Science Letters 53, 189–202.

Eidam, J., Hammer, J., Korich, D., Bielicki, K.-H., 1995. Amphibole-bearing granites in the Lusatian Anticlinal Zone: Variscan I-type magmatism at the margin of the Bohemian Massif. Neues Jahrbuch für Mineralogie - Abhandlungen 168, 259–281.

Eidam, J., Krauss, M., Hammer, J., Korich, D., 2001. Zur Ausbildung und zum Alter der zonalen kataklastisch-mylonitischen Deformation im Lausitzer Granodioritkomplex. Zeitschrift für Geologische Wissenschaften 29, 471–481.

Feng, G., Weiming, F., Yuejun, W., Ming, Z., 2004. Origin of the early Cretaceous calc-alkaline lamprophyres from the Sulu orogen in eastern China: implications for enrichments process beneath continental collision belts. Lithos 78, 291–305.

Finger, F., Roberts, M.B., Haunschmid, B., Schermaier, A., Steyrer, H.B., 1997. Variscan granitoids of central Europe: their typology, potential sources and tectonothermal relations. Mineralogy and Petrology 61, 67–96.

Foley, S.F., 1992. Vein-plus-wall-rock melting mechanisms in the lithosphere and the origin of potassic alkaline magmas. Lithos 28, 435–453.

Förster, H.-J., Romer, R.L., 2010. Carboniferous magmatism. In: Linnemann, U. (Ed.), Pre-Mesozoic Geology of Saxo-Thuringia: From the Cadomian Active Margin to the Variscan Orogen, Schweizerbart, pp. 287–308.

Franke, W., 2000. The mid-European segment of the Variscides: tectonostratigraphic units, terrane boundaries and plate tectonic evolution. In: Franke, W., Haak, V., Oncken, O., Tanner, D. (Eds.), Orogenic Processes: Quantification and Modelling in the Variscan Belt: Geol. Soc., London, Spec. Publ., 179, pp. 35–61.

Hauri, E.H., Hart, S.R., 1997. Rhenium abundances and systematics in oceanic basalts. Chemical Geology 139, 185–205.

Hawthorne, F.C., Oberti, R., 2007. Amphiboles: crystal chemistry. Reviews in Mineralogy and Geochemistry 67, 1–54.

Hegner, E., Kolbl-Ebert, M., Loeschke, J., 1998. Post collisional Variscan lamprophyres (Black Forest, Germany). $^{40}Ar/^{39}Ar$ phlogopite dating, Nd, Pb, Sr isotope and trace element characteristics. Lithos 45, 395–411.

Heinrich, C., 1993. Hydrothermalmetamorphose und Geoschemie der Lausitzer Gabbronorit-Gabbro-Diorit Serie. Dissertation, Karlsruhe; 190 S.

Heuse, T., Blumenstengel, H., Elicki, O., Geyer, G., Hansch, W., Maletz, J., Sarmiento, G.N., Weyer, D., 2010. Biostratigraphy—the faunal province of the southern margin of the Rheic ocean. In: Linnemann, U., Romer, R.L. (Eds.), Pre-Mesozoic Geology of Saxo-Thuringia. From the Cadomian Active Margin to the Variscan Orogen Schweizerbart, Stuttgart, pp. 99–170.

Hoch, M., Rehkamper, M., Tobschall, H.J., 2001. Sr, Nd, Pb and O isotopes of minettes from Schirmacher Oasis, East Antarctica. A case of mantle metasomatism involving subducted continental material. Journal of Petrology 42, 1387–1400.

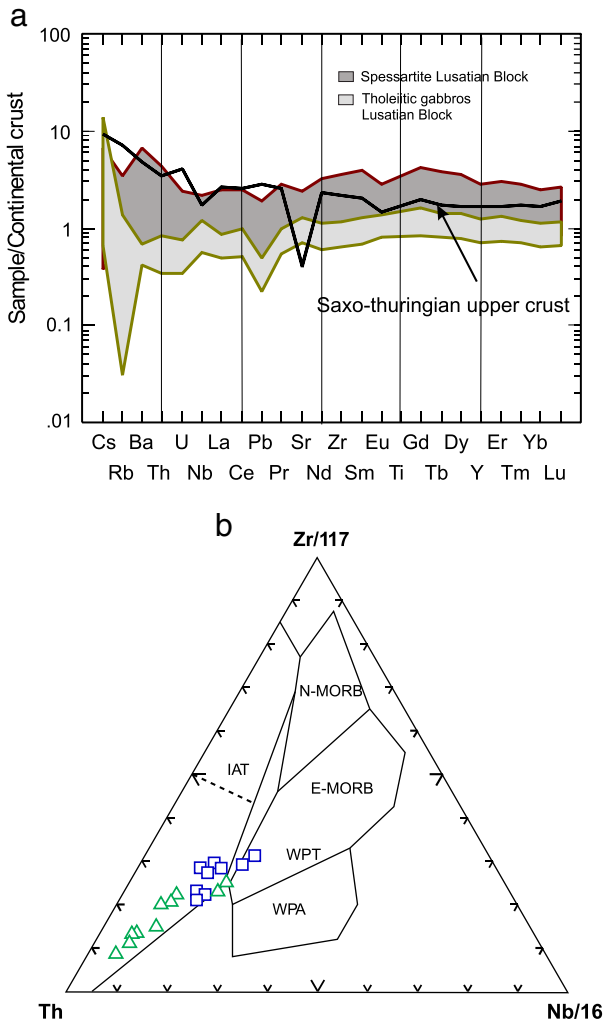

Fig. 10. (a) Continental crust-normalized patterns (Taylor and McLennan, 1985), and (b) Th–Zr–Nb discrimination diagram; N-MORB: normal-type mid-oceanic ridge basalt; E-MORB (WPT): enriched mid-oceanic ridge basalt (within-plate tholeiite); WPA: within-plate alkali; and IAT; island-arc tholeiite (Wood, 1980). The two samples in WPT are olivine gabbros.
Data sources are as in Figs. 6 and 9.

Hofmann, A.W., 1988. Chemical differentiation of the earth: the relationship between mantle, continental crust, and oceanic crust. Earth and Planetary Science Letters 90, 297–314.

Irvine, N., Baragar, W.R.A., 1971. A guide to chemical classification of the common volcanic rocks. Canadian Journal of Earth Sciences 8, 523–548.

Ishizuka, O., 1998. Vertical and horizontal variations of the fast neutron flux in a single irradiation capsule and their significance in the laser-heating $^{40}Ar/^{39}Ar$ analysis. Case study for the hydraulic rabbit facility of the JMTR reactor, Japan. Geochemical Journal 32, 243–252.

Ishizuka, O., Uto, K., Yuasa, M., Hochstaedter, A.G., 2002. Volcanism in the earliest stage of back-arc rifting in the Izu-Bonin arc revealed by laser-heating $^{40}Ar/^{39}Ar$ dating. Journal of Volcanology and Geothermal Research 120, 71–85.

Ito, E., White, W.M., Göpel, C., 1987. The O, Sr, Nd and Pb isotope geochemistry of MORB. Chemical Geology 62, 157–179.

Janoušek, V., Holub, F.V., 2007. The causal link between HP–HT metamorphism and ultrapotassic magmatism in collisional orogens: case study from the Moldanubian Zone of the Bohemian Massif. Proceedings of The Geologists Association 118, 75–86.

Janoušek, V., Holub, F., Magna, T., Erban, V., 2010. Isotopic constraints on the petrogenesis of the Variscan Ultrapotassic magmas from Moldanubian Zone of the Bohemian massif. Mineralogia Special Paper 37, 32–36.

Jones, A.P., Smith, J.V., 1983. Petrological significance of mineral chemistry in the Agaltha peak and the thumb minettes, Navajo volcanic field. Journal of Geology 91, 643–656.

Kemnitz, H., 2007. The Lausitz graywackes, Saxo-Thuringia, Germany — witness to the Cadomian orogeny. In: Linnemann, U., Nance, R.D., Kraft, P., Zulauf, G. (Eds.), The Evolution of Rheic Ocean: From Avalonin–Cadomian Active Margin to Alleghenian–Variscan Collision: Geol. Soc. Am., Spec. Pap., 423, pp. 97–141.

Kemnitz, H., Romer, R.L., Oncken, O., 2002. Gondwana break-up and the northern margin of the Saxothuringian belt (Variscides of Central Europe). International Journal of Earth Sciences 91, 246–259.

Kindermann, A., Fiedler, F., Seifert, T., Uhlig, S., 2003. Platinmetall-Führung der Ni-Cu-Sulfidmineralisationen im Bereich der Lausitzer Antiklinalzone. Zeitschrift für Angewandte Geologie 49, 43–47.

Kramer, W., 1976. Zur Petrologie und Metallogenetischen Bedeutung der Dolerite (Lamprophyre) des Lausitzer Massivs. Zeitschrift für Geologische Wissenschaften 4, 975–994.

Kramer, W., 1988. Magmengenetische Aspekte der Lithosphärenentwicklung-Geochemich-petrologische Untersuchung basaltoider variszischer Gesteins-Formationen sowie mafischer und ultramafischer Xenolithe im nordöstlichen Zentraleuropa. Schriftenreihe für geologische Wissenschaften 26, 1–136.

Kramer, W., Andrehs, G., 2011. Basische Gangintrusionen im Oberlausitzer Bergland, Ostsachsen. Berichte der Naturforschenden Gesellschaft der Oberlausitz 19, 21–46.

Kramer, W., Müller, B., Peschel, A., 1977. Zur tektonischen und substantiellen Charakteristik der Basite des Lausitzer Antiklinoriums und deren Altersbeziehung. Zeitschrift für Geologische Wissenschaften 5, 95–100.

Krmíček, L., 2010. Pre-Mesozoic lamprophyres and lamproites of the Bohemian Massif (Czech Republic, Poland, Germany, Austria). Mineralogia Special Paper 37, 37–46.

Kroner, U., Goerz, I., 2010. Variscan assembling of the allochthonous domain of the Saxo-Thuringian Zone—a tectonic model. In: Linnemann, U., Romer, R.L. (Eds.), Pre-Mesozoic Geology of Saxo-Thuringia—From the Cadomian Active Margin to the Variscan Orogen, Schweizerbart, Stuttgart, pp. 271–286.

Kroner, U., Romer, R.L., 2010. The Saxo-Thuringian Zone-tip of the Armorican Spur and part of the Gondwana plate. In: Linnemann, U., Romer, R.L. (Eds.), Pre-Mesozoic Geology of Saxo-Thuringia. From the Cadomian Active Margin to the Variscan Orogen, Schweizerbart, pp. 371–394.

Kroner, U., Hahn, T., Romer, R.L., Linnemann, U., 2007. The Variscan orogeny in the Saxo-Thuringian Zone — heterogenous overprint of Cadomian/Paleozoic Peri-Gondwana crust. Geological Society of America Special Papers 423, 153–172.

Kroner, U., Mansy, J.L., Mazur, S., Aleksandrowski, P., Hann, H.P., Huckriede, H., Lacquement, F., Lamarche, J., Ledru, P., Pharao, T.C., Zedler, H., Zeh, A., Zuulauf, G., 2008. Variscan tectonics. In: McCann, T. (Ed.), The Geology of Central Europe: Geol. Soc. Lond. , pp. 599–664.

Kroner, U., Romer, R.L., Linnemann, U., 2010. The Saxo-Thuringian Zone of the Variscan Orogen as part of Pangea. In: Linnemann, U., Romer, R.L. (Eds.), Pre-Mesozoic Geology of Saxo-Thuringia. From the Cadomian Active Margin to the Variscan Orogen Schweizerbart, Stuttgart, pp. 3–16.

Kryza, R., Pin, C., 2010. The Central-Sudetic ophiolites (SW Poland): petrogenetic issues, geochronology and palaeotectonic implications. Gondwana Research 17, 292–305.

Lanphere, M.A., Baadsgaard, H., 2001. Precise K–Ar, $^{40}Ar/^{39}Ar$, Rb–Sr, U/Pb mineral ages from the 27.5 Ma Fish Canyon Tuff reference standard. Chemical Geology 175, 653–671.

Le Maitre, R.W., Bateman, P., Dudek, A., Keller, J., Lameyre, J., Le Bas, M.J., Sabine, P.A., Schmid, R., Sorensen, H., Streickeisen, A., Wooley, A.R., Zanetten, B., 2002. Igneous Rocks: a Classification and Glossary of Terms: Recommendations of the International Union of Geological Sciences Subcommission on the Systematics of Igneous Rocks. Cambridge University Press, Cambridge . 236 pp.

Letterrier, J., Maury, R.C., Thonon, P., Girard, D., Marchal, M., 1982. Clinopyroxene composition as a method of identification of the magmatic affinities of paleo-volcanic series. Earth and Planetary Science Letters 59, 139–154.

Lindsley, D.H., 1983. Pyroxene thermometry. American Mineralogist 68, 477–493.

Linnemann, U., Romer, R.L., 2002. The Cadomian orogeny in Saxo-Thuringia, Germany: geochemical and Nd–Sr–Pb isotopic characterization of marginal basins with constraints to geotectonic setting and provenance. Tectonophysics 352, 33–64.

Linnemann, U., Gehmlich, M., Tichomirowa, M., Buschmann, B., Nasdala, L., Jonas, P., Lützner, H., Bombach, K., 2000. From Cadomian subduction to Early Palaeozoic rifting. The evolution of Saxo-Thuringia at the margin of Gondwana in the light of single zircon geochronology and basin development (central European Variscides, Germany). In: Franke, W., Haak, V., Oncken, O., Tanner, D. (Eds.), Orogenic Processes: Quantification and Modelling in the Variscan Belt: Geol. Soc. Lond., Spec. Publ., 179, pp. 131–153.

Linnemann, U., McNaughton, N.J., Romer, R.L., Gehmlich, M., Drost, K., Tonk, C., 2004. West Africa provenance for Saxo-Thuringia (Bohemia Massif): did Armorica ever leave pre-Pangean Gondwana? — U/Pb-SHRIMP zircon evidence and the Nd-isotopic record. International Journal of Earth Sciences 93, 683–705.

Linnemann, U., Pereira, F., Jeffries, T.E., Drost, K., Gerdes, A., 2008. The Cadomian Orogeny and the opening of the Rheic Ocean. The diacrony of geotectonic processes constrained by LA–ICP-MS U–Pb zircon dating (Ossa-Morena and Saxo-Thuringian Zones, Iberian and Bohemian Massifs). Tectonophysics 461, 21–43.

Linnemann, U., Romer, R.L., Gerdes, A., Jeffries, T.E., Drost, K., Ulrich, J., 2010a. The Cadomian Orogeny in the Saxo-Thuringian Zone. In: Linnemann, U., Romer, R.L. (Eds.), Pre-Mesozoic Geology of Saxo-Thuringia. From the Cadomian Active Margin to the Variscan Orogen, Schweizerbart, pp. 37–58.

Linnemann, U., Hofmann, M., Romer, R.L., Gerdes, A., 2010b. Transitional stages between the Cadomian and Variscan orogenies: basin development and tectono-magmatic evolution of the southern margin of the Rheic Ocean at the Saxo-Thuringian Zone (North Gondwana shelf). In: Linnemann, U., Romer, R.L. (Eds.), Pre-Mesozoic Geology of Saxo-Thuringia. From the Cadomian Active Margin to the Variscan Orogen, Schweizerbart, pp. 59–99.

Macdonald, R., Thorpe, R.S., Gaskarth, J.W., Grindrod, A.R., 1985. Multi-component origin of Caledonian lamprophyres of northern England. Mineralogical Magazine 49, 485–494.

Matte, P., 1991. Accretionary history and crustal evolution of the Variscan belt in western Europe. Tectonophysics 196, 309–337.

Matte, P., 2001. The Variscan collage and orogeny (480–290 Ma) and the tectonic definition of the Armorica microplate: a review. Terra Nova 13, 122–128.

Mingram, B., 1998. The Erzgebirge, Germany — a subducted part of northern Gondwana: geochemical evidence for repetition of early Paleozoic metasedimentary sequences in metamorphic thrust. Geological Magazine 135, 785–801.
Morimoto, N., 1988. The nomenclature of pyroxenes. Mineralogical Magazine 52, 535–550.
Nédli, Zs, Tóth, T.M., 2007. Origin and geodynamic significance of Upper Cretaceous lamprophyres from the Villány Mts (Hungary). Mineralogy and Petrology 90, 73–107.
Oliver, G.J.H., Corfu, F., Krogh, T.E., 1993. U–Pb ages from SW Poland. Evidence for a Caledonian suture zone between Baltica and Gondwana. Journal of the Geological Society of London 150, 355–369.
Peschel, A., Müller, B., Kramer, W., 1973. Die basischen Intrusivgesteine der Lausitz und ihre industrielle Nutzung. Freiberger Forschungshefte H C 283, 1–153.
Pin, C., Majerowicz, A., Wojciechowska, I., 1988. Upper Paleozoic oceanic crust in the Polish Sudetes: Nd–Sr isotope and trace element evidence. Lithos 21, 195–209.
Plank, T., Langmuir, C.H., 1998. The chemical composition of subducting sediments and its consequences for the crust and mantle. Chemical Geology 145, 325–394.
Prelević, D., Foley, S.F., Cvetković, V., Romer, R.L., 2004. Origin of minette by mixing of lamproite and dacite magmas in Veliki Majdan, Serbia. Journal of Petrology 45, 759–792.
Prelević, D., Foley, S.F., Romer, R.L., Cvetković, V., Downes, H., 2005. Tertiary ultrapotassic volcanism in Serbia: constraints on petrogenesis and mantle source characteristics. Journal of Petrology 46, 1443–1487.
Prelević, D., Foley, S.F., Cvetković, V., 2007. A review of petrogenesis of Mediterranean Tertiary lamproites: a perspective from the Serbian ultrapotassic province. In: Beccaluva, L., Bianchini, G., Wilson, M. (Eds.), Cenozoic Volcanism in the Mediterranean Area: Geol. Soc. Am., Spec. Pap. 418, pp. 113–129.
Prelević, D., Akal, C., Romer, R.L., Foley, S.F., 2010. Lamproites as indicators of accretion and/or shallow subduction in the assembly of south-western Anatolia, Turkey. Terra Nova 22, 443–452.
Prelević, D., Akal, C., Foley, S.F., Romer, R.L., Stracke, A., van den Bogaard, P., 2012. Ultrapotassic mafic rocks as geochemical proxies for postcollisional mantle dynamics of lithosphere: the case of SW Anatolia, Turkey. Journal of Petrology 49, 1–37.
Renno, A.D., Stanek, K.P., Lobst, R., Pushkarev, Y., 2003a. A new lamprophyre species from the Klunst quarry (Ebersbach, Lusatia, Germany) — geochemical and petrological implications. Zeitschrift für Geologische Wissenschaften 31, 1–20.
Renno, A.D., Hacker, B.R., Stanek, K.P., 2003b. An Early Cretaceous (126 Ma) utramafic alkaline lamprophyre from the Quarry Klunst (Ebersbach, Lusatia, Germany). Zeitschrift für Geologische Wissenschaften 31, 31–36.
Rock, N.M.S., 1977. The nature and origin of lamprophyres: some definitions, distinctions and derivations. Earth-Science Reviews 13, 123–169.
Rock, N.M.S., 1991. Lamprophyres. Blackie & Son, Glasgow, pp. 43–46.
Romer, R.L., Hahne, K., 2010. Life of the Rheic Ocean: scrolling through the shale record. Gondwana Research 17, 236–253.
Romer, R.L., Heinrich, W., Schröder-Smeibidl, B., Meixner, A., Fischer, C.O., Schulz, C., 2005. Elemental dispersion and stable isotope fractionation during reactive fluid-flow and fluid immiscibility in the Bufa del Diente aureole, NE-Mexico. Evidence from radiographies and Li, B, Sr, Nd, and Pb isotope systematics. Contributions to Mineralogy and Petrology 149, 400–429.
Rötzler, K., Plessen, B., 2010. The Erzgebirge: a pile of ultrahigh- to low-pressure nappes of Early Palaeozoic rocks and their Cadomian basement. In: Linnemann, U., Romer, R.L. (Eds.), Pre-Mesozoic Geology of Saxo-Thuringia — From the Cadomian Active Margin to the Variscan Orogen, Schweizerbart, pp. 253–270.
Rudnick, R.L., Fountain, D.M., 1995. Nature and composition of the continental crust; a lower crustal perspective. Reviews of Geophysics 33, 267–309.
Seifert, Th, 2008. Metallogeny and Petrogenesis of Lamprophyres in the Mid-European Variscides: Post-collisional Magmatism and its Relationship to Late-Varsican Ore Forming Processes (Bohemian Massif). IOS Press BV, Amsterdam, Netherlands, pp. 1–128.
Stille, P., Oberhänsli, R., Wenger-Schenk, K., 1989. Hf–Nd isotopic and trace element constraints on the genesis of alkaline and calc-alkaline lamprophyres. Earth and Planetary Science Letters 96, 209–219.
Stosch, H.-G., Lugmair, G.W., 1990. Geochemistry and evolution of kyanite-bearing eclogites from the Münchberg massif, southern Germany. Earth and Planetary Science Letters 99, 230–249.
Sun, C.M., Bertrand, J., 1991. Geochemistry of clinopyroxenes in plutonic and volcanic sequences from the Yanbian Proterozoic ophiolites (Sichuan Province, China): petrogenetic and geotectonic implications. Schweizer Mineralogische Und Petrographische Mitteilungen 71, 243–259.
Sun, S.S., McDonough, W.F., 1989. Chemical and isotopic systematics of oceanic basalts: implications for the mantle composition and processes. In: Saunders, A.D., Norry, M.J. (Eds.), Magmatism in the Ocean Basins: Geol. Soc. Spec. Publ., 42, pp. 313–345.
Tappe, S., Foley, S.F., Kjarsgaard, B.A., Romer, R.L., Heaman, L.M., Stracke, A., Jenner, G.A., 2008. Between carbonatite and lamproite — Diamondiferous Torngat ultramafic lamprophyres formed by carbonatefluxed melting of cratonic MARID-type metasomes. Geochimica et Cosmochimica Acta 72, 3258–3286.
Taylor, S.R., McLennan, S.M., 1985. The Continental Crust: Its Composition and Evolution. Blackwell, Oxford. 312 pp.
Taylor, S.R., McLennan, S.M., 1995. The geochemical evolution of the continental crust. Reviews of Geophysics 33, 241–265.
Turpin, L., Velde, D., Pinte, G., 1988. Geochemical comparison between minettes and kersantites from the western European Hercynian orogen. trace element and Pb–Sr–Nd isotope constraints on their origin. Earth and Planetary Science Letters 87, 73–86.
Turpin, L., Cuney, M., Friedrich, M., Bouchez, J.L., Aubertin, M., 1990. Meta-igneous origin of Hercynian peraluminous granites in N–W French Massif Central: implications for crustal history reconstructions. Contributions to Mineralogy and Petrology 104, 163–172.
Uto, K., Ishizuka, O., Matsumoto, A., Kamioka, H., Togashi, K., 1997. Laser-heating $^{40}Ar/^{39}Ar$ dating system of the Geological Survey of Japan. System outline and preliminary results. Bulletin of the Geological Survey of Japan 48, 23–46.
von Seckendorff, V., Timmerman, M.J., Kramer, W., Wrobel, P., 2004. New $^{40}Ar/^{39}Ar$ ages and geochemistry of Late Carboniferous–early Permian lamprophyres and related volcanic rocks in the Saxothuringian Zone of the Variscan Orogen (Germany). In: Wilson, M., Neumann, E.R., Timmermann, G.R., Heremans, M., Larsen, B.T. (Eds.), Permo-Carboniferous Magmatism and Rifting in Europe: Geol. Soc. Lond. Spec. Pub., 223, pp. 335–359.
Wenzel, T., Mercolli, I., Oberhänsli, R., 1991. The plutonic rocks of the Meissen Massif (Germany): evidence for open and closed system fractionation processes. Schweizer Mineralogische Und Petrographische Mitteilungen 71, 371–390.
Wood, D.A., 1980. The application of a Th–Hf–Ta diagram to problems of tectonomagmatic classification and establishing the nature of crustal contamination of basaltic lavas of the British Tertiary volcanic province. Earth and Planetary Science Letters 50, 11–30.
Workman, R.K., Hart, S.R., 2005. Major and trace element composition of the depleted MORB mantle (DMM). Earth and Planetary Science Letters 231, 53–72.
Zartman, R.L., Doe, B.R., 1981. Plumbotectonics—the model. Tectonophysics 75, 135–162.
Zindler, A., Hart, S., 1986. Chemical geodynamics. Annual Review of Earth and Planetary Sciences 14, 493–571.
Zuleger, E., Erzinger, J., 1988. Determination of REE and Y in silicate materials with ICP-AES. Fresenius Zeitschaft fur Analytische Chemie 332, 140–143.